Phytocytokine signaling integrates cell surface immunity and nitrogen limitation

Jakub Rzemieniewski[1], Henriette Leicher[1], Hyun Kyung Lee[2], Caroline Broyart[2], Shahran Nayem[3], Christian Wiese[1,†], Julian Maroschek[1], Zeynep Camgöz[1], Vilde Olsson Lalun[4], Michael Anthony Djordjevic[5], A. Corina Vlot[3,‡], Ralph Hückelhoven[1], Julia Santiago[2] and Martin Stegmann[1*]

[1]Phytopathology, TUM School of Life Sciences, Technical University of Munich, Freising, Germany

[2]The Plant Signaling Mechanisms Laboratory, Department of Plant Molecular Biology, University of Lausanne, Lausanne, Switzerland

[3]Helmholtz Zentrum Munich, Institute of Biochemical Plant Pathology, Neuherberg, Germany

[4]Section for Genetics and Evolutionary Biology, Department of Biosciences, University of Oslo, Oslo, Norway

[5]Division of Plant Science, Australian National University, Acton, Canberra, Australia

[†]present address: Botany, TUM School of Life Sciences, Technical University of Munich, Freising, Germany

[‡]present address: Chair of Crop Plant Genetics, Faculty of Life Sciences: Food, Nutrition and Health, University of Bayreuth, Kulmbach, Germany

*Corresponding author: Email: martin.stegmann@tum.de

Abstract

Little is known about plant genetic and biochemical components that coordinate immune responses with growth and environmental cues. C-TERMINALLY ENCODED PEPTIDEs (CEPs) control plant development and nitrogen demand signaling. Here, we identified CEP4 as an immune-modulatory peptide (phytocytokine) in *Arabidopsis thaliana*. CEP4 and related CEPs are important regulators of resistance to plant pathogenic bacteria and are perceived by the tissue-specific receptor kinases CEP RECEPTOR 1 (CEPR1), CEPR2 and the phylogenetically related RECEPTOR-LIKE KINASE 7 (RLK7). CEP4 promotes flagellin-triggered responses and we provide evidence that CEPs modulate cell surface immunity upon N limitation. We propose that CEPs integrate biotic and abiotic stress-associated signals to safeguard plant health.

Introduction

Receptor kinases (RKs) sense external and internal cues to control multiple aspects of plant physiology. RKs can serve as pattern recognition receptors (PRRs) to detect microbe-associated molecular patterns (MAMPs) and activate pattern-triggered immunity (PTI). An example is the *Arabidopsis thaliana* (hereafter Arabidopsis) leucine-rich repeat RK (LRR-RK) FLAGELLIN SENSITIVE 2 (FLS2), which forms a receptor complex with BRASSINOSTEROID INSENSITIVE 1-ASSOCIATED RK 1 (BAK1) upon perception of a 22 amino acid epitope derived from bacterial flagellin (flg22) to activate PTI (*1*). Plants also perceive endogenous peptides that plants release during infection or MAMP recognition. These peptides are referred to as phytocytokines and are also perceived by RKs. They modulate immunity but often also plant growth and development (*2*, *3*). In many cases, phytocytokines are transcriptionally induced upon MAMP

perception, but this is not a prerequisite for their function, as previously shown for GLV2 (*4–7*). Phytocytokines and other endogenous peptides regulate several abiotic stress responses, including adaptation to high salinity, drought and nutrient deprivation, suggesting that they might integrate multiple external and internal cues to safeguard plant health (*8–10*). Yet, information is sparse on plant cell surface components with functions in more than one peptide-mediated pathway. C-TERMINALLY ENCODED PEPTIDES (CEPs) are important for sucrose-dependent lateral root growth, root system architecture, systemic nitrogen (N)-demand signaling and promotion of root nodulation, but a role in plant immunity remained unknown (*8*, *11–15*). Here, we studied CEPs as new phytocytokines in Arabidopsis and discovered a function in adaptation of immune responses to N availability.

Results

CEPs are novel phytocytokines

Screening of public transcript abundance data identified a specific member of the CEP family, *CEP4*, that showed differential flg22-induced expression (Fig. S1A) (*16*). RT-qPCR confirmed flg22-dependent downregulation of *CEP4* expression in Col-0 roots (Fig. S1B). CEPs are produced as peptide precursors and contain one to five CEP domains that require maturation for peptide release (*17*). To test for CEP4 involvement in immunity, we generated CEP4 precursor overexpression lines (*35S*::*CEP4*, Fig. S2A) which were more resistant to *Pseudomonas syringae* pv. *tomato (Pto)* lacking the chemical effector molecule coronatine (*Pto*$^{COR-}$) (Fig. 1A). Arabidopsis encodes 12 class I CEPs including CEP4 which has a distinctive sequence (*18*). CEP4 only carries two proline residues in its peptide domain and the second proline is positioned uniquely compared to other classical class I CEPs with three prolines (e.g. CEP1 and CEP3) (Table S1). Most previously identified CEPs are 15mers with an N-terminal aspartate (D), a C-terminal histidine (H) and hydroxylated prolines (*8*). We tested whether a 16mer CEP4 with proline hydroxylation (Hyp), DAFRHypTHQGHypSQGIGH, triggers immune responses. CEP4 induced dose-dependent PTI signaling outputs, including cellular influx of calcium ions in Col-0 expressing the calcium reporter aequorin (Col-0^{AEQ}), activation of MITOGEN-ACTIVATED PROTEIN KINASEs (MAPKs), ethylene production and expression of the PTI marker gene *FLAGELLIN-INDUCED RECEPTOR KINASE 1* (*FRK1*) (Fig. 1B-E, Fig. S3A). CEP4 also induced YFP fluorescence in the vasculature of *pFRK1::NLS-3xmVenus* seedlings (*19*) (Fig. 1F), seedling growth inhibition (SGI) and systemic resistance to *Pto* (Fig. 1G,H). The 15mer CEP4 (AFRHypTHQGHypSQGIGH) triggered dose-dependent calcium influx similar to the 16mer (Fig. S3A). CEP1 and CEP9.5 (Table S1) also triggered significant calcium influx in seedlings, but only at high concentrations (10 µM) (Fig. S3B). CEP1 further induced YFP fluorescence in the vasculature of *pFRK1::NLS-3xmVenus* lines (Fig. S3C). We confirmed a role for class I CEPs in plant immunity by generating a *cep6x* hextuple mutant by CRISPR-Cas9 in which we mutated CEP4, CEP1-CEP3, CEP6 and CEP9 (Fig. S2B,C). The *cep6x* mutant showed compromised resistance to both *Pto*$^{COR-}$ and *Pto* wild type, demonstrating that CEPs are important for antibacterial resistance (Fig. 1I, Fig. S2D). The *cep6x* susceptibility phenotype was complemented with *35S::CEP4* (Fig. 1J, Fig. S2E).

Class I CEPs predominantly express in root tissue (*17*) and function as systemic root-to-shoot transmitters of N starvation (*8*). We hypothesized that root-expressed *CEPs* regulate leaf immunity upon *Pto* infection. Reciprocal grafts between *cep6x* and Col-0 showed, however, that *CEP* mutation in the shoot conferred increased *Pto* susceptibility (Fig. S4A). We detected *CEP1-CEP4*, *CEP6* and *CEP9* expression in leaf tissue using RT-qPCR and imaging *pCEP4::NLS-3xmVENUS* reporter plants (Fig. S4B,C) with *CEP4* being slightly upregulated upon *Pto* infection (Fig. S4B). The *CEP4* promoter showed activity in seedling leaf tissue but not in the vasculature (Fig. S4D). Consistent with previous reports, *CEP4* expressed in emerging lateral roots (Fig. S4C) (*17*). Given that CEP4 induced *FRK1* expression in the vasculature (Fig. 1F, S3C), it is possible that CEP4 is mobile between different tissue layers of the leaf.

CEPR1 and CEPR2 are CEP4 receptors and central regulators of plant immunity

CEPs bind to CEPR1 and CEPR2, two LRR-RLKs from subfamily XI (*8*). We resolved expression patterns of *CEPR1* and *CEPR2* in leaf tissues using *pCEPR1::NLS-3xmVenus* and *pCEPR2::NLS-3xmVenus* lines. As expected, *CEPR1* expressed in vasculature tissue (Fig. 2A), as previously reported (*8*), whereas *CEPR2* was largely restricted to stomatal guard cells (Fig. 2A). We tested whether *CEPR1* and *CEPR2* control immunity. Single *cepr1-3* or *cepr2-4* mutants did not show a *Pto*$^{COR-}$ infection phenotype (Fig. 2B, S5A,B). However, *cepr1-3 cepr2-4 (cepr1-3/2-4*) and a CRISPR-Cas9 *cepr1 cepr2* double mutant in Col-0^{AEQ} (*cepr1/2*^{AEQ}) were both more susceptible to *Pto*$^{COR-}$ (Fig. 2B, S5A). These data suggest that *CEPR1* and *CEPR2* spatially complement each other to control *Pto*$^{COR-}$ resistance.

We tested whether CEP4 perception depends on CEPR1 and/or CEPR2. Using SGI as a readout, *cepr1-3* was insensitive and two *cepr2* alleles (*cepr2-3* and *cepr2-4*) were insensitive and less sensitive to CEP4 treatment, respectively (Fig. S6A,B). The *cepr1-3/2-4* mutant and No-0 *cepr1-1 cepr2-1* double mutant did also not respond to CEP4 (Fig. 2C, Fig. S6C). Similarly, the *cepr1-3/2-4* mutant was insensitive to CEP4-induced systemic resistance (Fig. 2D). These data suggest that both CEPR1 and CEPR2 mediate CEP4 perception.

We then tested whether CEP4 binds to purified insect cell-expressed ectodomains (ECDs) of CEPR1 and/or CEPR2. We analyzed protein quality by Coomassie stain and size exclusion chromatography (SEC, Fig. S7A,B). Unfortunately, CEPR1^{ECD} aggregated, as indicated by the early elution of the bulk sample during SEC analysis (~8 mL corresponding to the column void volume, Fig. S7A). By contrast, isothermal titration calorimetry (ITC) showed that CEPR2^{ECD}, which eluted with a single SEC peak at ~13 mL (Fig. S7A,B), directly bound CEP4 with a K_D of 15.7 µM (± 4.5 µM) (Fig. 2E, H, Fig. S7C). A scrambled control (CEP4^{scr}) did not bind to CEPR2^{ECD} (Fig. 2F, H, Fig. S7C). CEP1, which was previously shown to bind to CEPR1 and CEPR2 (*8*), also bound to CEPR2^{ECD} with a K_D of 9.3 µM (± 0.6 µM) (Fig. 2G,H, Fig. S7C). These data are in range with previously reported peptide-LRR-RK binding affinities obtained by ITC and suggest that CEPR2 is a CEP4 receptor (*20–23*).

We tested whether *CEPR1* and *CEPR2* were important for FLS2-mediated PTI. We did not observe strong differences in flg22-induced ethylene accumulation in *cepr1-3/2-4* (Fig. S8A). Of note, flg22-induced ethylene production was higher in *cepr1-3/2-4*, but basal ethylene production was also enhanced, making

117 the result difficult to interpret. However, we found that flg22-induced *FRK1* and *PR1* expression was
118 strongly reduced in *cepr1-3/2-4* and reduced in *cepr1-3* and *cepr2-4* (Fig. 2I). The flg22-induced seedling
119 growth inhibition was not affected in *cepr1-3/2-4* (Fig. S8B), suggesting that CEPR1/CEPR2 are selectively
120 required for specific flg22-induced outputs. We also tested whether CEP-CEPR1/2 signaling was important
121 for systemic acquired resistance (SAR). Local inoculation of *Pto* avrRPM1 and subsequent infection of
122 systemic tissue with virulent *Pto* (*24*) revealed that *cepr1-3/2-4* and *cep6x* were strongly compromised in
123 *Pto* avrRPM1-triggered SAR (Fig. 2J). Collectively, these data show that CEP-CEPR signaling is a central
124 regulator of plant immunity in Arabidopsis.
125
126 **RLK7 is a novel CEP4-specific CEP receptor**
127 To further characterize the role of CEPR1 and CEPR2 in CEP4 signaling, we tested early CEP4-induced
128 responses in *cepr1-3/2-4* and *cepr1/2*^{AEQ}. Surprisingly, we found that *cepr1/2*^{AEQ} did not show compromised
129 calcium influx upon CEP4 treatment (Fig. 3A). CEP4-induced MAPK activation was also unaffected in
130 *cepr1-3/2-4* (Fig. 3B). Moreover, *cepr1-3* and *cepr2-4* showed mildly reduced CEP4-induced *FRK1*
131 expression, which was more pronounced, but not abolished, in *cepr1-3/2-4* (Fig. 3C). These results
132 suggested that other receptor(s) are involved in CEP4 perception. CEPR1 and CEPR2 are phylogenetically
133 close to IKU2, which is involved in seed size regulation, and RLK7 which controls germination speed, lateral
134 root formation and salt stress adaptation (*10*, *25–27*). RLK7 also senses endogenous PAMP-INDUCED
135 PEPTIDES (PIPs) to regulate resistance to the fungal vascular pathogen *Fusarium oxysporum* and *Pto*
136 (*28*, *29*). The *iku2-4* mutant showed unaltered CEP4-induced ethylene accumulation, but the response was
137 strongly compromised in *rlk7-1* and *rlk7-3* (Fig. S9A). CEP4-induced ethylene production was also impaired
138 in *cepr1-3/2-4*, but the results are difficult to interpret given the mutant´s high basal ethylene accumulation
139 (Fig. S9B). Similarly, *rlk7-1* and *rlk7-3* showed strongly reduced CEP4-induced MAPK activation (Fig. 3D).
140 We also generated a *rlk7/iku2*^{AEQ} mutant (Fig. S5C) which showed strongly compromised CEP4-induced
141 calcium influx (Fig. 3E). CEP4-induced *FRK1* expression was mildly affected in *rlk7-1* and *rlk7-3,* similar to
142 *cepr1-3/2-4* (Fig. 3F,C). These data suggest that RLK7 also functions as a CEP4 receptor. Interestingly,
143 *rlk7-1* and *rlk7-3* were only moderately affected in CEP4-induced SGI (Fig. 3G), suggesting that CEP4
144 activates distinct responses via specific receptors. Moreover, CEP1-induced calcium influx was abolished
145 in *cepr1/2*^{AEQ} and unaltered *in rlk7/ iku2*^{AEQ}, indicating that CEPR1/2 are required for canonical class I CEP-
146 mediated early immune signaling responses (Fig. 3H).
147 We used ITC to test whether CEP4 binds to RLK7^{ECD}. Similar to CEPR2^{ECD}, we obtained good quality
148 proteins for RLK7^{ECD} eluting with a main single SEC peak at ~13 mL (Fig. S7A,B). CEP4 bound to RLK7^{ECD}
149 with a K_D of 9 µM (± 4.9 µM) (Fig. 3I,L, Fig. S7), like CEPR2^{ECD} (Fig. 2E,H). We also tested binding of PIP1,
150 a defined RLK7 ligand, to RLK7^{ECD} (*10*, *28*). RLK7^{ECD} bound PIP1 with higher affinity (K_D 500 nM ± 60 nM)
151 (Fig. 3J,L, S7C). Importantly, consistent with unaltered CEP1-induced responses in *rlk7/iku2*^{AEQ} (Fig. 3H),
152 CEP1 did not bind to RLK7 (Fig. 3K,L Fig. S7C). Collectively, these data suggest that RLK7 can also
153 function as a CEP4-specific CEP receptor. By analyzing a *pRLK7::Venus-H2B*, we found wide-spread

154 expression of *RLK7* which overlapped with *CEP4* in aerial parts of seedlings (Fig. 3M, S4C). This suggests
155 that CEP4 and RLK7 meet *in vivo* to function as a receptor-ligand pair.
156
157 **CEPs promote FLS2 signaling during N starvation**

158 Class I *CEP* expression, including *CEP4*, is not strongly affected by flg22 treatment or *Pto* infection (Fig.
159 S1A,B, S4B). We were thus interested to determine the biological context of CEP-mediated control of
160 immunity. We tested whether CEP4 treatment also affects FLS2-dependent signaling. CEP4 promoted
161 flg22-induced ethylene accumulation and resistance induced by a low dose of flg22 (100 nM) (Fig. 4A,B).
162 Yet, we did not observe defects in flg22-induced MAPK activation and *FRK1* expression in *cep6x* (Fig.
163 4C,D). Several *CEPs* are transcriptionally upregulated in N-starved roots, including *CEP1* (*8*). Similarly,
164 *CEP4* was transcriptionally upregulated upon N limitation of seedlings (Fig. 4E). The N status of plants
165 affects disease resistance to different pathogens, but the underlying molecular mechanisms remain
166 unknown (*30*). N starvation promoted resistance to *Pto*, suggesting a connection between N homeostasis
167 and antibacterial resistance (*31*). We thus hypothesized that CEPs coordinate the plant´s N status with cell
168 surface immunity. We N-deprived two-week-old seedlings for 24 h by transferring them to ½ MS medium
169 with low N content (10% N concentration of ½ MS medium, low N). Upon elicitation, wild type seedlings
170 showed enhanced flg22-triggered MAPK activation and *FRK1* expression (Fig 4F,G). This N status-
171 dependent promotion of flg22-triggered PTI was abolished in *cep6x.* These data suggest that CEPs
172 contribute to FLS2-dependent signaling under N limited conditions. Moreover, flg22 stimulated expression
173 of the high affinity *NITRATE TRANSPORTER 2.1 (NRT2.1)* (*32*) upon N limitation in a *CEP*-dependent
174 manner (Fig. 4H). Together, these results indicate a tight CEP-dependent connection between PTI and N
175 availability, highlighting signaling cross-talk between cell surface immunity and the plant`s nutritional status.
176
177 **Discussion**
178
179 This work reveals that CEP perception is achieved by three partially tissue-specific receptors that regulate
180 plant immunity and likely coordinate biotic stress with plant nutritional cues. The close overlap of *CEP4* and
181 *RLK7* expression in leaves, but not with *CEPR1* and *CEPR2*, suggests a combination of cell autonomous
182 and short distance signaling contributing to CEP-mediated immune modulation. A challenge for the future
183 will be to determine how three CEP receptors with distinct expression patterns integrate responses between
184 tissues and the concerted action of diverse ligands. RLK7 also recognizes endogenous PIPs, likely with
185 higher affinity over CEP4 (*26*, *28*). Members of the CLE peptide family also bind multiple receptors with
186 variable binding affinities to regulate epidermal cell patterning (*22*, *33*). Dissecting spatiotemporal ligand
187 availability and CEP4-PIP1 signaling specificity will be an important future task. RLK7 does not bind to
188 CEP1, but CEP4, suggesting that CEP4`s receptor specificities are unique among CEPs, likely caused by
189 its distinct sequence. It will be interesting to compare the molecular mechanism of PIP1/CEP4-RLK7 and
190 CEP1/CEP4-CEPR2/CEPR1 recognition in future structure analyses. Plant peptides may be versatile tools

191 for the evolution of plant plasticity. Increasing ligand and receptor diversity may provide vast combinations
192 for fine-tuned signal outputs.
193 Our data suggest that N starvation facilitates CEP expression to promote flg22 responsiveness. Other
194 phytocytokines modulate immune signaling by regulating PRR abundance or receptor complex formation
195 and dynamics, but in most cases the mechanism remains unknown (*3*, *7*, *34*, *35*). It will be interesting to
196 reveal whether CEPs directly or indirectly modulate PRR signalling.
197 Recent evidence suggests a direct integration of nutrient homeostasis and PTI in plants. Perception of
198 flg22 induces PHT1.4 phosphorylation to inhibit phosphate (Pi) uptake and promote root immunity (*36*).
199 CEPs induce nitrate, Pi and sulfate uptake, suggesting CEP-CEPR1/CEPR2/RLK7-dependent transporter
200 modulation (*37*). NRT transport activity can be regulated by kinases, including phosphorylation of NRT1.2
201 by CEPR2, which we identified as a CEP4 receptor (*38*, *39*). Since N starvation promotes CEP-dependent
202 PTI, it is also possible that sufficient N dampens immune signaling via a yet unknown mechanism. This
203 may be important in ecological or agronomic contexts, when plants need to decide whether to invest into
204 defense or growth depending on nutrient availability.
205 CEP signaling also regulates sucrose-dependent root growth inhibition and fecundity (*14*, *40*), placing
206 CEPs as central integrators of biotic stress with plant nutrition, growth and development (*37*).
207 CEPR1/CEPR2/RLK7 and CEPs are widely conserved among angiosperms, including crop plants (*41*).
208 CEPs are important to promote nodulation in legumes (*42*, *43*). It will be critical to understand whether N-
209 dependent and CEP-mediated promotion of PTI extends beyond Arabidopsis and to decipher how CEPs
210 can both promote immunity and control symbiosis in diverse species. This will provide important insights
211 for future crop improvement strategies that coordinate crop nutrition with disease resistance.
212
213 **Materials and methods**
214
215 Molecular cloning
216 To generate *CEP4* overexpression lines, the coding sequence of *CEP4* (AT2G35612) was synthesized
217 (Twist Bioscience, USA) with attB attachment sites for subsequent gateway cloning into pDONRZeo
218 (Invitrogen, USA) and recombination with pB7WG2 (VIB, Ghent). To generate CRISPR-Cas9 mutants,
219 appropriate target sites (two per gene of interest) were designed using the software tool chopchop
220 (https://chopchop.cbu.uib.no/). Individual guide RNA constructs containing gene specific target sites were
221 synthesized (Twist Bioscience, USA) and subsequently stacked in a GoldenGate-adapted pUC18-based
222 vector (45). To generate *cep6x*, *cepr1/2*^{AEQ} and *rlk7/iku2*^{AEQ}, 12, 4 and 4 target site-containing gRNA
223 constructs were stacked, respectively (Table 2). Together with FastRed-pRPS5::Cas9, higher order gRNA
224 stacks were subsequently cloned into pICSL4723 for in planta expression (46).
225 To generate the *pCEP4::NLS-3xmVenus*, *pCEPR1::NLS-3xmVenus* and *pCEPR2::NLS-3xmVenus*
226 reporter constructs, 1000, 1696 and 2788 bp fragments upstream of the start codon, respectively, were
227 amplified from genomic DNA and assembled together with the sequence coding for the nuclear localization
228 signal of SV40 large T antigen followed by 3 consecutive mVenus YFP fluorophores (47) into a GoldenGate-

229 modified pCB302 binary vector for plant expression. For p*RLK7* the 1957 bp promoter sequence upstream
230 from the start codon was amplified with primers containing attB attachment sites for subsequent gateway
231 cloning into pDONRZeo (Invitrogen, USA) and recombination with promotor::Venus (YFP)-H2B destination
232 vector (56). All of the generated plant expression constructs were subsequently transformed into
233 *Agrobacterium tumefaciens* strain GV3101 before floral dip transformation of Arabidopsis. All primers used
234 for cloning are listed in Table S3.
235
236 Plant material and growth conditions
237 Arabidopsis Col-0, Col-0^{AEQ} and No-0 were used as wild types for experiments and generation of transgenic
238 lines or CRISPR mutants (48). The *cepr1-3* (GK-467C01), *cepr2-3* (SALK_014533), *rlk7-1* (SALK_056583),
239 *rlk7-3* (SALK_120595), *iku2-4* (Salk_073260) and the novel *cepr2*-4 allele (GK-695D11) were obtained from
240 NASC (UK) (14, 28, 49, 50) . The No-0 *cepr2-1xcepr2-1* was obtained from RIKEN (Japan) (8). T-DNA
241 insertion mutants were genotyped by PCR using T-DNA- and gene-specific primers as listed in Table S3.
242 The lack of *CEPR2* transcript in *cepr2-4* (GK-695D11) was determined by semi-quantitative PCR from
243 cDNA using *cepr2-4* genotyping primers (Fig. S5B). The *cepr1-3/2-4* double mutant was obtained by
244 genetic crossing. The *bak1-5/bkk1* mutant was characterized previously (51). For visualizing tissue-specific
245 *FRK1* expression, a *pFRK1::NLS-3xmVenus* line was used (19). To isolate homozygous CRISPR mutants,
246 pICSL4723 transformant T1 seeds showing red fluorescence were selected and grown on soil before
247 genotyping with gene specific primers and Sanger sequencing (Table 3). Mutants lacking the transgene
248 were identified by loss of fluorescence. To generate the *cep6x p35S::CEP4* lines, pB7WG2 CEP4 was used
249 for floral dip transformation of homozygous *cep6x*.
250 Plants for physiological assays involving mature plants were vernalized for 2-3 days in the dark at 4°C and
251 later grown in individual pots in environmentally controlled growth rooms (20-21°C, 55% relative humidity,
252 8 h photoperiod). For seedling-based assays, seeds were sterilized using chlorine gas and grown axenically
253 on ½ Murashige and Skoog (MS) media supplemented with vitamins (Duchefa, Netherlands), 1% sucrose,
254 with or without 0.8% agarose at 22°C and a 16 h photoperiod unless stated otherwise. For experiments
255 using N depleted ½ MS medium, modified MS salts without nitrogen-containing compounds (Duchefa,
256 Netherlands) were used and supplemented with KNO_3/NH_4NO_3 to achieve 100% N (KNO_3 9.395 mM,
257 NH_4NO_3 10.305 mM) and 10% N (KNO_3 0.9395 mM, NH_4NO_3 1.0305 mM) conditions. To keep the ionic
258 strength equal in 10% N conditions, the medium was supplemented with 90% KCl (8.455 mM).
259
260 Grafting
261 Arabidopsis seedlings were grown vertically on ½ MS agar medium without sucrose in short day conditions
262 seven days before grafting. Grafting was performed aseptically under a stereo microscope as previously
263 described (52). Vertically mounted plates with reciprocally grafted seedlings were returned to short-day
264 conditions for 10 days. Healthy seedlings were transferred to soil.
265
266

267 Imaging and microscopy

268 Confocal laser-scanning microscopy was performed using a Leica TCS SP5 (Leica, Germany) microscope
269 (with Leica Application Suite X 3.7.4.23463) and all the pictures were taken with a 20x water immersion
270 objective. For the mVenus fluorophore, pictures were imaged with argon laser excitation at 514nm and a
271 detection window of 525-535 nm. Propidium iodide was visualized using DPSS 561 laser emitting at 561
272 nm with a detection window of 575-590 nm. For imagining the expression pattern of NLS-3xmVenus or
273 Venus (YFP)-H2B under the control of different promoters (*pCEP4*, *pCEPR1*, *pCEPR2* and *pRLK7*),
274 vertically-grown seedlings were stained with propidium iodide immediately before microscopic analysis. For
275 imagining the *pFRK1::NLS-3xmVenus* reporter line, 12-day old seedlings were transferred to a 24-well-
276 plate containing ddH_2O with or without (mock) peptides in the indicated concentrations. For comparison of
277 *FRK1* promoter activity, seedlings were analysed by confocal microscopy using identical laser intensities
278 and interval/number of slices for Z stack projection 16 h after treatment.
279

280 Calcium influx assay

281 Apoaequorin-expressing liquid-grown eight-day-old seedlings were transferred individually to a 96-well
282 plate containing 100 µl of 5 µM coelenterazine-h (PJK Biotech, Germany) and incubated in the dark
283 overnight. Luminescence was measured using a plate reader (Luminoskan Ascent 2.1, Thermo Fisher
284 Scientific, USA). Background luminescence was recorded by scanning each well 12 times at 10 s intervals,
285 before adding a 25 µl elicitor solution to the indicated final concentration. Luminescence was recorded for
286 30 min at the same interval. The remaining aequorin was discharged using 2 M $CaCl_2$, 20% ethanol. The
287 values for cytosolic Ca^{2+} concentrations ($[Ca^{2+}]_{cyt}$) were calculated as luminescence counts per second
288 relative to total luminescence counts remaining (L/L_{max}).
289

290 Ethylene measurement

291 Leaf discs (4 mm in diameter) from four-to-five-week-old soil-grown Arabidopsis were recovered overnight
292 in ddH_2O. Three leaf discs per sample were transferred to a glass vial containing 500 µl of ddH_2O before
293 adding ddH_2O (mock) or peptides to the indicated final concentration. Glass vials were capped with a rubber
294 lid and incubated under gentle agitation for 3.5 h. One mL of the vial headspace was extracted with a
295 syringe and injected into a Varian 3300 gas chromatograph (Varian, USA) to measure ethylene.
296

297 MAPK activation

298 Five-day old Arabidopsis seedlings growing on ½ MS agar plates, were transferred into a 24-well plate
299 containing liquid medium for seven days. 24 h before the experiment, seedlings were equilibrated in a fresh
300 ½ MS medium. For N depletion experiments modified ½ MS containing 100% N or 10% N supplemented
301 with 90% KCl was used. MAPK activation was elicited by adding the peptides to the indicated
302 concentrations. Six seedlings per sample were harvested, frozen in liquid nitrogen and homogenized using
303 a tissue lyser (Qiagen, Germany). Proteins were extracted using a buffer containing 50 mM Tris-HCl (pH
304 7.5), 50 mM NaCl, 10% glycerol, 5 mM DTT, 1% protease inhibitor cocktail, 1 mM phenylmethylsulfonyl

305 fluoride (PMSF), 1% IGEPAL, 10 mM EGTA, 2 mM NaF, 2 mM Na_3VO_4, 2 mM Na_2MoO_4, 15 mM ß-
306 Glycerophosphate and 15 mM p-nitrophenylphosphate before analysis by SDS-PAGE and western blot.
307 Phosphorylated MAPKs were detected by α-p44/42 antibodies (Cell Signaling, USA).
308
309 Seedling growth inhibition
310 Arabidopsis seedlings were grown for five days on ½ MS agar plates, before transfer of individual seedlings
311 into each well of a 48-well plate containing liquid medium with or without elicitors in the indicated
312 concentration. After seven-day treatment, fresh weight of individual seedlings was measured.
313
314 Pathogen growth assay
315 *Pseudomonas syringae* pv. *tomato* (*Pto)* DC3000 and *Pto* lacking the effector molecular coronatine *Pto*$^{COR-}$
316 were grown on King's B agar plates containing 50 µg/mL rifampicin and 50 µg/mL kanamycin at 28ºC. After
317 two-to-three days bacteria were resuspended in ddH_2O containing 0.04% Silwet L77 (Sigma Aldrich, USA).
318 The bacterial suspension was adjusted to an OD_{600} = 0.2 (10^8 cfu/mL) for *Pto*$^{COR-}$ or OD_{600} = 0.02 (10^7
319 cfu/mL) for *Pto* DC3000 before spray inoculating four-to-five-week-old plants. For peptide-induced
320 resistance in local tissues, ddH_2O (mock), flg22 (100 nM) and/or CEP4 (1 µM) were syringe-infiltrated into
321 mature leaves. After 24 h, *Pto* DC3000 (OD_{600} = 0.0002, 10^5 cfu/mL) was syringe-infiltrated into pre-treated
322 leaves and incubated for three days before determining bacterial counts. For CEP4-induced resistance in
323 systemic tissues, CEP4 (1 µM) or ddH_2O (mock) were syringe-infiltrated into the first two true leaves of
324 young three-to-four-week-old Arabidopsis. After three days, *Pto* DC3000 (OD_{600}=0.0002, 10^5 cfu/mL) was
325 syringe-infiltrated into leaves three and four of the pre-treated plants. Bacterial counts were determined four
326 days after infection.
327
328 Systemic acquired resistance
329 SAR experiments were performed as previously described (53). Briefly, plants were cultivated in a mixture
330 of substrate (Floradur) and silica sand in a 5:1 ratio under short day (SD) conditions (10 h) in a growth
331 chamber at 22 °C /18 °C (day/night) with a light intensity of 100 µmol $m^{-2}s^{-1}$, and 70% relative humidity
332 (RH). SAR assays were performed using *Pto* DC3000 and *Pto* AvrRpm1. Bacteria were grown on NYGA
333 media (0.5% peptone, 0.3% yeast extract, 2% glycerol, 1.8% agar, 50 µg/mL kanamycin, 50 µg/mL
334 Rifampicin) at 28° C before infiltration. Freshly grown *Pto* avrRpm1 was diluted in 10 mM $MgCl_2$ (to reach
335 a final concentration of 1×10^6 cfu/mL) and syringe-infiltrated in the first two true leaves of four-and-a-half-
336 week-old plants. Concurrently, 10 mM $MgCl_2$ was applied to a separate set of plants as the mock control
337 treatment. Three days after *Pto* avrRpm1 infiltration, plants were challenged in their 3rd and 4th leaves with
338 *Pto* DC3000 (1×10^5 cfu/mL). Bacterial titers were determined four days after *Pto* DC3000 infection.
339
340 Gene expression analysis
341 For seedlings-based assays, 12-day-old liquid-grown seedlings were equilibrated in fresh medium for 24 h
342 before treatment with the indicated peptides. For adult plants, four-to-five-week-old Arabidopsis leaves

343 were syringe-infiltrated with ddH_2O (mock), flg22 (1 µM) or *Pto* DC3000 (OD_{600} = 0.001, $5x10^5$ cfu/mL) and
344 incubated for 24 h. All samples for RT-qPCR analysis were harvested at the indicated time points, frozen
345 in liquid nitrogen and homogenized using a tissue lyser (Qiagen, Germany). Total RNA was isolated using
346 TRIzol reagent (Roche, Switzerland) and purified using Direct-zol™ RNA Miniprep Plus kit (Zymo
347 Research, Germany). 2 µg of the total RNA was digested with DNase I and reverse transcribed with oligo
348 (dT)18 and Revert Aid reverse transcriptase. RT-qPCR experiments were performed using Maxima SYBR
349 green mix (Thermo Fisher Scientific, USA) with the AriaMx Real-Time PCR system (Agilent Technologies,
350 USA). Expression levels of all tested genes were normalized to the house-keeping gene *Ubiquitin 5* (*UBQ5*).
351 Sequences of all primers used for RT-qPCR analysis are found in Table S3.
352
353 Expression and purification of recombinant receptor ectodomains
354 *Spodoptera frugiperda* codon-optimized synthetic genes (Invitrogen GeneArt), coding for Arabidopsis
355 CEPR1 (residues 23 to 592), CEPR2 (residues 32 to 620) and RLK7 (residues 29 to 608) were cloned into
356 a modified pFastBAC vector (Geneva Biotech) providing a 30K signal peptide (54), a C-terminal TEV
357 (tobacco etch virus protease) cleavable site and a StrepII-9xHis affinity tag. For protein expression,
358 *Trichoplusia ni Tnao38* cells (55) were infected with CEPR1, CEPR2 or RLK7 virus with a multiplicity of
359 infection (MOI) of 3 and incubated one day at 28°C and two days at 21°C at 110 rounds per minute (rpm).
360 The secreted proteins were purified by Ni^{2+} (HisTrap excel, Cytiva, equilibrated in 25 mM KP_i pH 7.8 and
361 500 mM NaCl) followed by Strep (Strep-Tactin Superflow high-capacity, IBA Lifesciences, equilibrated in
362 25 mM Tris pH 8.0, 250 mM NaCl, 1 mM EDTA) affinity chromatography. All proteins were incubated with
363 TEV protease to remove the tags. Proteins were purified by SEC on a Superdex 200 Increase 10/300 GL
364 column (Cytiva, USA) equilibrated in 20 mM citrate pH 5.0, 150 mM NaCl and further concentrated using
365 Amicon Ultra concentrators from Millipore (Merck, Germany) with a 30,000 Da molecular weight cut-off.
366 Purity and structural integrity of the different proteins were assessed by SDS-PAGE.
367
368 Analytical size-exclusion (SEC) chromatography
369 Analytical SEC experiments were performed using a Superdex 200 Increase 10/300 GL column (GE, USA).
370 The columns were pre-equilibrated in 20 mM citric acid pH 5, 150 mM NaCl. 150 µg of CEPR1, CEPR2 and
371 RLK7 were injected sequentially onto the column and eluted at 0.5 mL/min. Ultraviolet absorbance (UV) at
372 280 nm was used to monitor the elution of the proteins. The peak fractions were analyzed by SDS-PAGE
373 followed by Coomassie blue staining.
374
375 Isothermal titration calorimetry (ITC)
376 Experiments were performed at 25°C on a MicroCal PEAQ-ITC (Malvern Instruments, UK) using a 200 µL
377 standard cell and a 40 µL titration syringe. CEP1, CEP4, $CEP4^{scr}$ and PIP1 peptides were dissolved in the
378 SEC buffer to match the receptor protein. A typical experiment consisted of injecting 1 µL of a 300 µM
379 solution of the peptide into 30 µM CEPR2 or RLK7 solution in the cell at 150 s intervals. ITC data were
380 corrected for the heat of dilution by subtracting the mixing enthalpies for titrant solution injections into

protein-free ITC buffer. Experiments were done in duplicates and data were analyzed using the MicroCal PEAQ-ITC Analysis Software provided by the manufacturer. The N values were fitted to 1 in the analysis.

Synthetic peptides

The flg22 peptide was kindly provided by Dr. Justin Lee (IPB Halle). Other peptides were synthesized by Pepmic (China) with at least 90% purity and dissolved in ddH_2O. Sequences of all the synthetic peptides can be found in Table S1.

Quantification and statistical analysis

Statistical analyses were performed using GraphPad Prism (Version 9.4.1). Sample size, p-values and statistical methods employed are described in the respective figure legends.

Data and material availability

All data are available in the main text or the supplementary materials. All newly generated mutant lines are available upon request to M.S.

References

1. B. P. M. Ngou, P. Ding, J. D. G. Jones, Thirty years of resistance: Zig-zag through the plant immune system. *Plant Cell*. **34**, 1447–1478 (2022).
2. A. A. Gust, R. Pruitt, T. Nürnberger, Sensing danger: Key to activating plant immunity. *Trends Plant Sci.* **22**, 779–791 (2017).
3. J. Rzemieniewski, M. Stegmann, Regulation of pattern-triggered immunity and growth by phytocytokines. *Curr. Opin. Plant Biol.* **68**, 102230 (2022).
4. K. Gully, S. Pelletier, M.-C. C. Guillou, M. Ferrand, S. Aligon, I. Pokotylo, A. Perrin, E. Vergne, M. Fagard, E. Ruelland, P. Grappin, E. Bucher, J.-P. P. Renou, S. Aubourg, The SCOOP12 peptide regulates defense response and root elongation in Arabidopsis thaliana. *J. Exp. Bot.* **70**, 1349–1365 (2019).
5. J. Rhodes, A.-O. Roman, M. Bjornson, B. Brandt, P. Derbyshire, M. Wyler, M. Schmid, F. L. H. Menke, J. Santiago, C. Zipfel, Perception of a conserved family of plant signalling peptides by the receptor kinase HSL3. *Elife*. **11**, e74687 (2022).
6. Z. Liu, S. Hou, O. Rodrigues, P. Wang, D. Luo, K. Nomura, C. Yin, H. Wang, W. Zhang, K. Zhu-salzman, Phytocytokine signalling reopens stomata in plant immunity and water loss. *Nature*. **605**, 332–339 (2022).
7. M. Stegmann, P. Zecua-Ramirez, C. Ludwig, H.-S. Lee, B. Peterson, Z. L. Nimchuk, Y. Belkhadir, R. Hückelhoven, RGI-GOLVEN signalling promotes cell surface immune receptor abundance to regulate plant immunity. *EMBO Rep.* **23**, e53281 (2022).
8. R. Tabata, K. Sumida, T. Yoshii, K. Ohyama, H. Shinohara, Y. Matsubayashi, Perception of root-derived peptides by shoot LRR-RKs mediates systemic N-demand signaling. *Science*. **346**, 343–346 (2014).
9. F. Takahashi, T. Suzuki, Y. Osakabe, S. Betsuyaku, Y. Kondo, N. Dohmae, H. Fukuda, K. Yamaguchi-Shinozaki, K. Shinozaki, A small peptide modulates stomatal control via abscisic acid in long-distance signalling. *Nature*. **556**, 235–238 (2018).

423 10. H. Zhou, F. Xiao, Y. Zheng, G. Liu, Y. Zhuang, Z. Wang, Y. Zhang, J. He, C. Fu, H. Lin, PAMP-
424 INDUCED SECRETED PEPTIDE 3 modulates salt tolerance through RECEPTOR-LIKE KINASE 7
425 in plants. *Plant Cell*. **34**, 927–944 (2021).

426 11. K. Ohyama, M. Ogawa, Y. Matsubayashi, Identification of a biologically active, small, secreted
427 peptide in Arabidopsis by in silico gene screening, followed by LC-MS-based structure analysis.
428 *Plant J.* **55**, 152–160 (2008).

429 12. M. Taleski, N. Imin, M. A. Djordjevic, CEP peptide hormones: Key players in orchestrating
430 nitrogen-demand signalling, root nodulation, and lateral root development. *J. Exp. Bot.* **69**, 1829–
431 1836 (2018).

432 13. C. Delay, K. Chapman, M. Taleski, Y. Wang, S. Tyagi, Y. Xiong, N. Imin, M. A. Djordjevic, CEP3
433 levels affect starvation-related growth responses of the primary root. *J. Exp. Bot.* **70**, 4763–4774
434 (2019).

435 14. K. Chapman, M. Taleski, H. A. Ogilvie, N. Imin, M. A. Djordjevic, CEP-CEPR1 signalling inhibits
436 the sucrose-dependent enhancement of lateral root growth. *J. Exp. Bot.* **70**, 3955–3967 (2019).

437 15. S. Roy, L. M. Müller, A rulebook for peptide control of legume – microbe endosymbioses. *Trends*
438 *Plant Sci.* **27**, 870–889 (2022).

439 16. B. Li, S. Jiang, X. Yu, C. Cheng, S. Chen, Y. Cheng, J. S. Yuan, D. Jiang, P. He, L. Shan,
440 Phosphorylation of Trihelix Transcriptional Repressor ASR3 by MAP KINASE4 Negatively
441 Regulates Arabidopsis Immunity. *Plant Cell*. **27**, 839–856 (2015).

442 17. I. Roberts, S. Smith, B. De Rybel, J. Van Den Broeke, W. Smet, S. De Cokere, M. Mispelaere, I.
443 De Smet, T. Beeckman, The CEP family in land plants: Evolutionary analyses, expression studies,
444 and role in Arabidopsis shoot development. *J. Exp. Bot.* **64**, 5371–5381 (2013).

445 18. C. Delay, N. Imin, M. A. Djordjevic, CEP genes regulate root and shoot development in response
446 to environmental cues and are specific to seed plants. *J. Exp. Bot.* **64**, 5383–5394 (2013).

447 19. L. Poncini, I. Wyrsch, V. D. Tendon, T. Vorley, T. Boller, N. Geldner, J. P. Métraux, S. Lehmann, In
448 roots of Arabidopsis thaliana, the damage-associated molecular pattern AtPep1 is a stronger
449 elicitor of immune signalling than flg22 or the chitin heptamer. *PLoS One*. **12**, e0185808 (2017).

450 20. J. Santiago, B. Brandt, M. Wildhagen, U. Hohmann, L. A. Hothorn, M. A. Butenko, M. Hothorn,
451 Mechanistic insight into a peptide hormone signaling complex mediating floral organ abscission.
452 *Elife*. **5**, 1–19 (2016).

453 21. J. Rhodes, H. Yang, S. Moussu, F. Boutrot, J. Santiago, C. Zipfel, Perception of a divergent family
454 of phytocytokines by by the Arabidopsis receptor kinase MIK2. *Nat. Commun.* **12**, 5494 (2021).

455 22. P. Qian, W. Song, T. Yokoo, A. Minobe, G. Wang, T. Ishida, S. Sawa, J. Chai, T. Kakimoto, The
456 CLE9/10 secretory peptide regulates stomatal and vascular development through distinct
457 receptors. *Nat. Plants*. **4**, 1071–1081 (2018).

458 23. S. Hou, D. Liu, S. Huang, D. Luo, Z. Liu, Q. Xiang, P. Wang, R. Mu, Z. Han, S. Chen, J. Chai, L.
459 Shan, P. He, The Arabidopsis MIK2 receptor elicits immunity by sensing a conserved signature
460 from phytocytokines and microbes. *Nat. Commun.* **12**, 5494 (2021).

461 24. H. H. Breitenbach, M. Wenig, F. Wittek, L. Jordá, A. M. Maldonado-Alconada, H. Sarioglu, T.
462 Colby, C. Knappe, M. Bichlmeier, E. Pabst, D. Mackey, J. E. Parker, A. Corina Vlot, Contrasting
463 roles of the apoplastic aspartyl protease APOPLASTIC, ENHANCED DISEASE
464 SUSCEPTIBILITY1-DEPENDENT1 and LEGUME LECTIN-LIKE PROTEIN1 in Arabidopsis
465 systemic acquired resistance. *Plant Physiol.* **165**, 791–809 (2014).

466 25. M. Luo, E. S. Dennis, F. Berger, W. J. Peacock, A. Chaudhury, MINISEED3 (MINI3), a WRKY
467 family gene, and HAIKU2 (IKU2), a leucine-rich repeat (LRR) KINASE gene, are regulators of
468 seed size in Arabidopsis. *Proc. Natl Acad. Sci. USA*. **102**, 17531–17536 (2005).

469 26. K. Toyokura, T. Goh, H. Shinohara, A. Shinoda, Y. Kondo, Y. Okamoto, T. Uehara, K. Fujimoto, Y.
470 Okushima, Y. Ikeyama, K. Nakajima, T. Mimura, M. Tasaka, Y. Matsubayashi, H. Fukaki, Lateral
471 inhibition by a peptide hormone-receptor cascade during Arabidopsis lateral root founder cell

472 formation. *Dev. Cell*. **48**, 64-75.e5 (2019).

473 27. D. Pitorre, C. Llauro, E. Jobet, J. Guilleminot, J. P. Brizard, M. Delseny, E. Lasserre, RLK7, a
474 leucine-rich repeat receptor-like kinase, is required for proper germination speed and tolerance to
475 oxidative stress in Arabidopsis thaliana. *Planta*. **232**, 1339–1353 (2010).

476 28. S. Hou, X. Wang, D. Chen, X. Yang, M. Wang, D. Turrà, A. Di Pietro, W. Zhang, The secreted
477 peptide PIP1 amplifies immunity through Receptor-Like Kinase 7. *PLoS Pathog.* **10**, e1004331
478 (2014).

479 29. S. Hou, H. Shen, H. Shao, PAMP-induced peptide 1 cooperates with salicylic acid to regulate
480 stomatal immunity in Arabidopsis thaliana. *Plant Signal. Behav.* **14**, 1666657 (2019).

481 30. M. Fagard, A. Launay, G. Clément, J. Courtial, A. Dellagi, M. Farjad, A. Krapp, M. C. Soulié, C.
482 Masclaux-Daubresse, Nitrogen metabolism meets phytopathology. *J. Exp. Bot.* **65**, 5643–5656
483 (2014).

484 31. C. Verly, A. C. R. Djoman, M. Rigault, F. Giraud, L. Rajjou, M. E. Saint-Macary, A. Dellagi, Plant
485 defense stimulator mediated defense activation is affected by nitrate fertilization and
486 developmental stage in Arabidopsis thaliana. *Front. Plant Sci.* **11**, 583 (2020).

487 32. D. Zhuo, M. Okamoto, J. J. Vidmar, A. D. M. Glass, Regulation of a putative high-affinity nitrate
488 transporter (Nrt2;1At) in roots of Arabidopsis thaliana. *Plant J.* **17**, 563–568 (1999).

489 33. A. Roman, P. Jimenez-sandoval, S. Augustin, C. Broyart, L. A. Hothorn, J. Santiago, HSL1 and
490 BAM1/2 impact epidermal cell development by sensing distinct signaling peptides. *Nat. Commun.*
491 **13**, 876 (2022).

492 34. M. Stegmann, J. Monaghan, E. Smakowska-Luzan, H. Rovenich, A. Lehner, N. Holton, Y.
493 Belkhadir, C. Zipfel, The receptor kinase FER is a RALF-regulated scaffold controlling plant
494 immune signaling. *Science*. **355**, 287–289 (2017).

495 35. J. Gronnier, C. M. Franck, M. Stegmann, T. DeFalco, A. Abarca, M. Von Arx, K. Duenser, W. Lin,
496 Z. Yang, J. Kleine-Vehn, C. Ringli, C. Zipfel, Regulation of immune receptor kinases plasma
497 membrane nanoscale landscape by a plant peptide hormone and its receptors. *Elife*. **11**, e74162
498 (2022).

499 36. J. Dindas, T. A. DeFalco, G. Yu, L. Zhang, P. David, M. Bjornson, M.-C. Thibaud, V. Custódio, G.
500 Castrillo, L. Nussaume, A. P. Macho, C. Zipfel, Direct inhibition of phosphate transport by immune
501 signaling in Arabidopsis. *Curr. Biol.* **32**, 488-495.e5 (2022).

502 37. S. Roy, M. Griffiths, I. Torres-Jerez, B. Sanchez, E. Antonelli, D. Jain, N. Krom, S. Zhang, L. M.
503 York, W. R. Scheible, M. Udvardi, Application of Synthetic Peptide CEP1 Increases Nutrient
504 Uptake Rates Along Plant Roots. *Front. Plant Sci.* **12**, 793145 (2022).

505 38. A. Jacquot, V. Chaput, A. Mauries, Z. Li, P. Tillard, C. Fizames, P. Bonillo, F. Bellegarde, E.
506 Laugier, V. Santoni, S. Hem, A. Martin, A. Gojon, W. Schulze, L. Lejay, NRT2.1 C-terminus
507 phosphorylation prevents root high affinity nitrate uptake activity in Arabidopsis thaliana. *New*
508 *Phytol.* **228**, 1038–1054 (2020).

509 39. L. Zhang, Z. Yu, Y. Xu, M. Yu, Y. Ren, S. Zhang, G. Yang, J. Huang, K. Yan, C. Zheng, C. Wu,
510 Regulation of the stability and ABA import activity of NRT1.2/NPF4.6 by CEPR2-mediated
511 phosphorylation in Arabidopsis. *Mol. Plant*. **14**, 633–646 (2021).

512 40. M. Taleski, K. Chapman, N. Imin, M. A. Djordjevic, M. Groszmann, The peptide hormone receptor
513 CEPR1 functions in the reproductive tissue to control seed size and yield. *Plant Physiol.* **182**, 620–
514 636 (2020).

515 41. C. Furumizu, A. K. Krabberød, M. Hammerstad, R. M. Alling, M. Wildhagen, S. Sawa, R. B. Aalen,
516 The sequenced genomes of nonflowering land plants reveal the innovative evolutionary history of
517 peptide signaling. *Plant Cell*. **33**, 2915–2934 (2021).

518 42. C. Laffont, A. Ivanovici, P. Gautrat, M. Brault, M. A. Djordjevic, F. Frugier, The NIN transcription
519 factor coordinates CEP and CLE signaling peptides that regulate nodulation antagonistically. *Nat.*
520 *Commun.* **11**, 3167 (2020).

521 43. Z. Luo, J. Wang, F. Li, Y. Lu, Z. Fang, M. Fu, K. S. Mysore, J. Wen, J. Gong, J. D. Murray, F. Xie,
522 The small peptide CEP1 and NIN-like protein NLP1 regulate NRT2.1 to mediate root nodule
523 formation across nitrate concentrations. *Plant Cell*. **in press** (2022).

524 44. C. Engler, R. Kandzia, S. Marillonnet, A one pot, one step, precision cloning method with high
525 throughput capability. *PLoS One*. **3**, e3647 (2008).

526 45. B. Castel, L. Tomlinson, F. Locci, Y. Yang, J. D. G. Jones, Optimization of T-DNA architecture for
527 Cas9-mediated mutagenesis in Arabidopsis. *PLoS One*. **14**, e0204778 (2019).

528 46. J. E. M. Vermeer, D. von Wangenheim, M. Barberon, Y. Lee, E. H. K. Stelzer, A. Maizel, N.
529 Geldner, A spatial accommodation by neighboring cells is required for organ initiation in
530 Arabidopsis. *Science*. **343**, 178–183 (2014).

531 47. M. Somssich, A. Bleckmann, R. Simon, Shared and distinct functions of the pseudokinase
532 CORYNE (CRN) in shoot and root stem cell maintenance of Arabidopsis. *J. Exp. Bot.* **67**, 4901–
533 4915 (2016).

534 48. M. R. Knight, A. K. Campbellt, S. M. Smith, A. J. Trewavas, Transgenic plant aequorin reports the
535 effects of touch and cold-shock and elicitors on cytoplasmic calcium. *Nature*. **314**, 524–526
536 (1991).

537 49. I. Dimitrov, F. E. Tax, Lateral root growth in Arabidopsis is controlled by short and long distance
538 signaling through the LRR RLKs XIP1/CEPR1 and CEPR2. *Plant Signal. Behav.* **13**, e1489667
539 (2018).

540 50. A. Fatihi, A. M. Zbierzak, P. Dörmann, Alterations in seed development gene expression affect
541 size and oil content of Arabidopsis seeds. *Plant Physiol.* **163**, 973–985 (2013).

542 51. M. Roux, B. Schwessinger, C. Albrecht, D. Chinchilla, A. Jones, N. Holton, F. G. Malinovsky, M.
543 Tör, S. de Vries, C. Zipfel, The Arabidopsis leucine-rich repeat receptor-like kinases BAK1/SERK3
544 and BKK1/SERK4 are required for innate immunity to hemibiotrophic and biotrophic pathogens.
545 *Plant Cell*. **23**, 2440–55 (2011).

546 52. C. W. Melnyk, Grafting with arabidopsis thaliana. *Methods Mol. Biol.* **1497**, 9–18 (2017).

547 53. M. Wenig, A. Ghirardo, J. H. Sales, E. S. Pabst, H. H. Breitenbach, F. Antritter, B. Weber, B.
548 Lange, M. Lenk, R. K. Cameron, J. P. Schnitzler, A. C. Vlot, Systemic acquired resistance
549 networks amplify airborne defense cues. *Nat. Commun.* **10**, 3183 (2019).

550 54. M. Futatsumori-Sugai, K. Tsumoto, Signal peptide design for improving recombinant protein
551 secretion in the baculovirus expression vector system. *Biochem. Biophys. Res. Commun.* **391**,
552 931–935 (2010).

553 55. Y. Hashimoto, S. Zhang, S. Zhang, Y. R. Chen, G. W. Blissard, Correction: BTI-Tnao38, a new
554 cell line derived from *Trichoplusia ni*, is permissive for AcMNPV infection and produces high levels
555 of recombinant proteins. *BMC Biotechnol.* **12** (2012).

556

557 **Author contributions**

558 Conceptualization: MS; Investigation: JR, HL, HKL, CB, SN, CW, JM, ZC, VOL, MS; Funding acquisition:
559 MS, JA, RH, ACV, MAD; Project administration: MS; Supervision: MS, JR, ACV, JS, MAD, RH; Writing –
560 original draft: MS, JR; Writing – review & editing: HL, HKL, CB, SN, CW, JM, VOL, MAD, ACV, RH, JS.

561 **Competing interests**

562 Authors declare that there are no competing interests.

563

564 **Acknowledgments**

565 We thank Stefanie Ranf for providing GoldenGate vectors for molecular cloning and Ulrich Hammes for
566 advice in grafting experiments. This work was funded by the following agencies: Deutsche
567 Forschungsgemeinschaft (DFG) grants STE2448/3-1 (MS and JR), STE2448/4-1 (MS and HL) and SFB924
568 TP B06 (ACV), the Technical University of Munich (MS, JR, RH, ZC, CW and JM), the Research Council
569 of Norway, Grant 230849 (VOL), Australian Research Council, Grant DP200101885 (MAD), the University
570 of Lausanne (CB), the Swiss National Science Foundation grants no. 310030_204526 and the European
571 Research Council (ERC) grant agreement no. 716358 (JS, HKL).

572

Figures

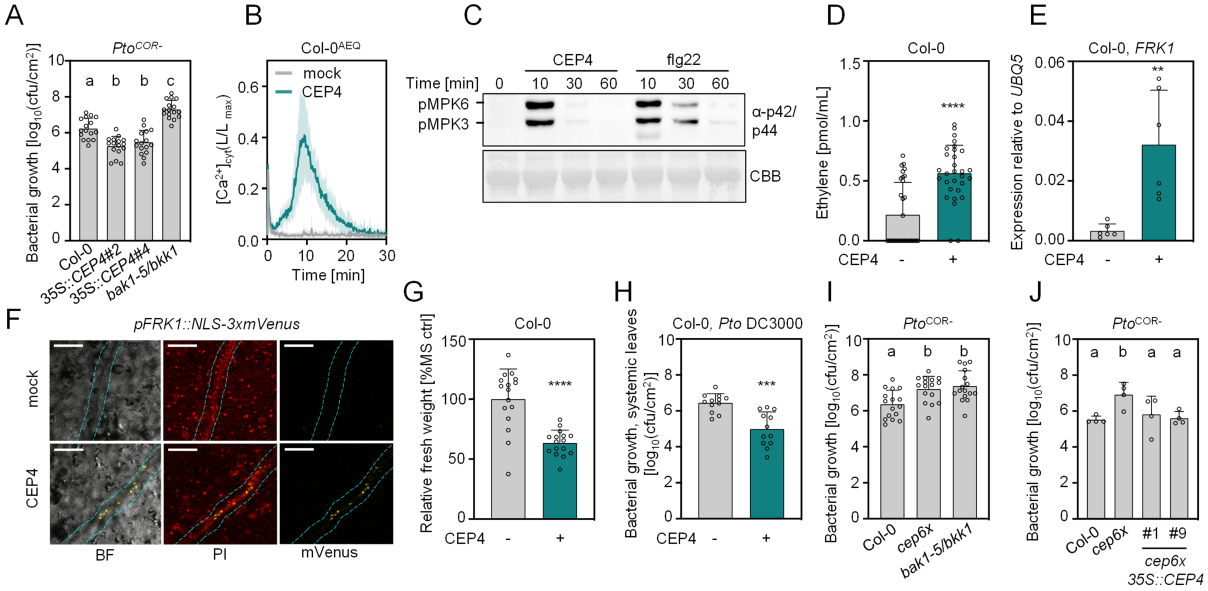

Figure 1: CEPs induce immune responses and are important determinants of plant immunity. A) Colony forming units (cfu) of *Pto*$^{COR-}$ 3 days post inoculation (3 dpi) upon spray infection; n = 16 pooled from four experiments ± SD (one-way ANOVA, Tukey post-hoc test; a-b, $p<0.01$; a/b-c $p<0.0001$) **B**) Kinetics of cytosolic calcium concentrations ($[Ca^{2+}]_{cyt}$) in Col-0^{AEQ} seedlings upon ddH_2O or CEP4 (1 µM) treatment; n = 8, ± SD. **C**) MAPK activation in Col-0 upon CEP4 (1 µM) or flg22 (100 nM) treatment. Western blots were probed with α-p44/42. CBB = Coomassie brilliant blue. **D**) Ethylene concentration in Col-0 leaf discs 3.5 h upon mock (ddH_2O) or CEP4 (1 µM) treatment; n = 30 pooled from six experiments ± SD (two-tailed Student's t-test, **** $p<0.0001$). **E**) RT-qPCR of *FRK1* in seedlings upon CEP4 (1 µM) or ddH_2O treatment for 4 h; n = 6 pooled from six experiments ± SD (two-tailed Student's t-test, ** $p<0.01$). Housekeeping gene *UBQ5*. **F**) NLS-3xmVenus signal in p*FRK1::NLS-3xmVenus* upon ddH_2O or CEP4 (1 µM) treatment for 16 h. Cyan dotted line indicates vasculature. BF = bright field, PI = propidium iodide, scale bar = 100 µm. **G**) Relative fresh weight of five-day-old seedlings treated with CEP4 (1 µM) for seven days (n=16, ± SD, **** $p<0.0001$, two-tailed Student's t-test). **H**) cfu of *Pto* DC3000 (4 dpi) in distal leaves upon local CEP4 (1 µM) or ddH_2O pre-treatment; n = 12 pooled from three experiment ± SD (two-tailed Student's t-test, *** $p=0.0001$). **I**) cfu of *Pto*$^{COR-}$ (3 dpi) upon spray infection; n = 16 pooled from four experiments ± SD (one-way ANOVA, Tukey post-hoc test, a-b $p\leq0.001$). **J**) cfu of *Pto*$^{COR-}$ (3dpi) upon spray infection; n = 4 ± SD (one-way ANOVA, Tukey post-hoc test, a-b $p<0.05$). All experiments were repeated at least three times in independent biological repeats with similar results.

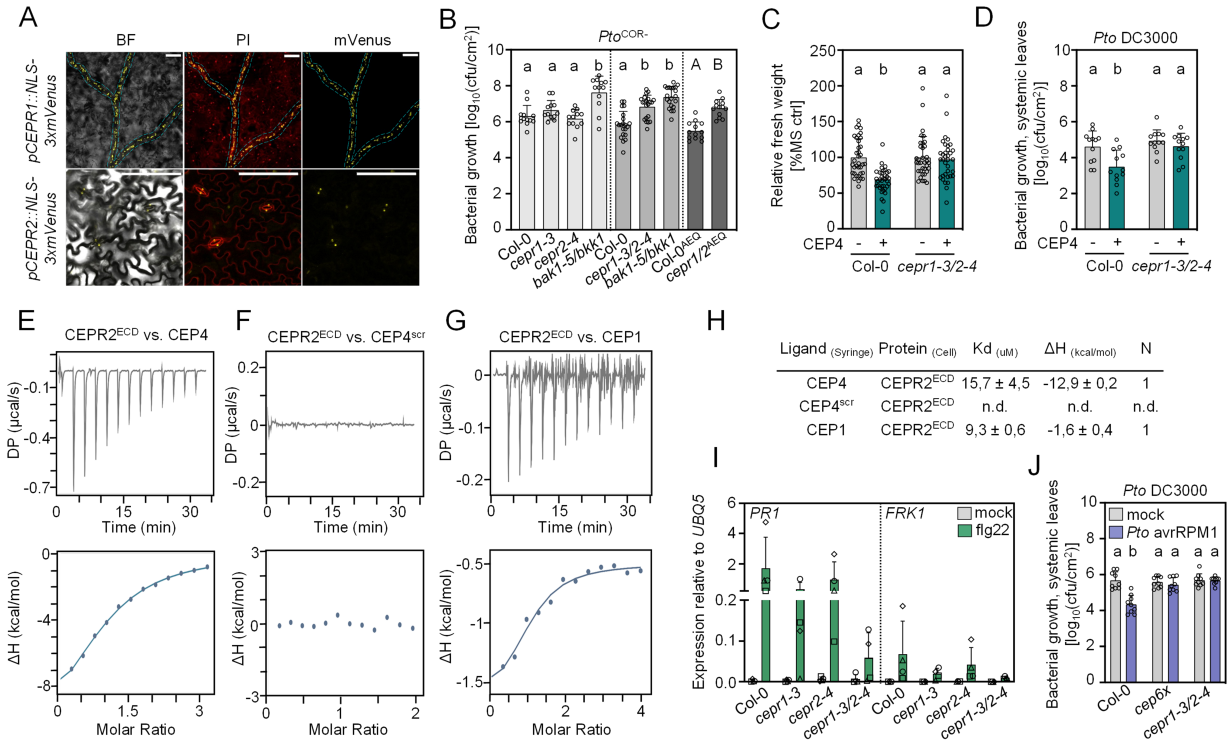

Ligand (Syringe)	Protein (Cell)	Kd (uM)	ΔH (kcal/mol)	N
CEP4	CEPR2^{ECD}	15,7 ± 4,5	-12,9 ± 0,2	1
CEP4^{scr}	CEPR2^{ECD}	n.d.	n.d.	n.d.
CEP1	CEPR2^{ECD}	9,3 ± 0,6	-1,6 ± 0,4	1

Figure 2: CEPR1 and CEPR2 are tissue-specific CEP4 receptors and important determinants of plant immunity. A) NLS-3xmVenus signal in the indicated lines. Cyan dotted line indicates vasculature. BF = bright field, PI = propidium iodide, scale bar = 100 µm. **B)** cfu of *Pto*$^{COR-}$ (3 dpi) upon spray infection. Dotted line indicates different experiments; n = 12, 21 and 13 pooled from three, five and three experiments, respectively ± SD (one-way ANOVA, Dunnett's post-hoc test, a-b p<0.0001, two-tailed Student's t-test, A-B p<0.0001). **C)** Relative fresh weight of five-days-old seedlings treated with CEP4 (1 µM) for seven days; n = 35-36 pooled from three experiments ± SD (one-way ANOVA, Tukey post-hoc test, a-b p<0.0001). **D)** cfu of *Pst* DC3000 (4 dpi) in distal leaves upon local CEP4 (1 µM) or ddH_2O pre-treatment; n = 12 pooled from three experiments ± SD (one-way ANOVA, Tukey post-hoc test, a-b p<0.01). **E)** CEP4, **F**) CEP4^{scr} and **G**) CEP1 were titrated into a solution containing CEPR2^{ECD} in ITC cells. Top: raw data thermogram; bottom: fitted integrated ITC data curves. **H)** ITC table summarizing CEPR2^{ECD} vs CEP4/CEP4^{scr}/CEP1 as means ± SD of two experiments. Dissociation constant (K_d) indicates receptor-ligand binding affinity. N indicates reaction stoichiometry (n = 1 for 1:1 interaction). **I)** RT-qPCR of *PR1* and *FRK1* in adult leaves after treatment with flg22 (100 nM) or ddH_2O for 24h; n = 4 ± SD. Housekeeping gene *UBQ5*. Different symbols represent four independent experiments. **J)** cfu of *Pto* DC3000 (4 dpi) in distal leaves upon local infection with *Pto avrRPM1* or 10 mM $MgCl_2$; n = 9 pooled from three independent experiments ± SD (one-way ANOVA, Tukey post-hoc test, a-b p<0.0001). Experiments in **A-D**, **I**, **J** and **E-G** were repeated at least three times in independent biological repeats or in two independent technical repeats, respectively, with similar results.

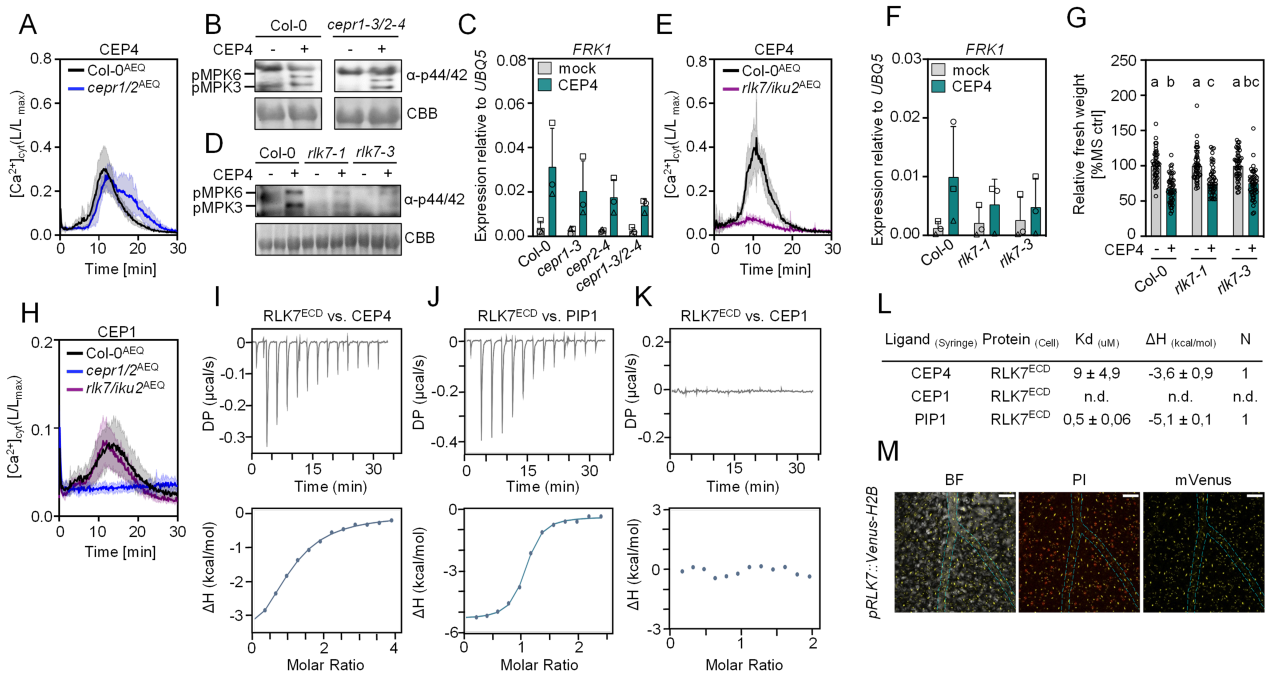

Ligand (Syringe)	Protein (Cell)	Kd (uM)	ΔH (kcal/mol)	N
CEP4	RLK7^{ECD}	9 ± 4,9	-3,6 ± 0,9	1
CEP1	RLK7^{ECD}	n.d.	n.d.	n.d.
PIP1	RLK7^{ECD}	0,5 ± 0,06	-5,1 ± 0,1	1

Figure 3: RLK7 is an additional CEP4 receptor. A) ($[Ca^{2+}]_{cyt}$) kinetics in seedlings upon CEP4 (1 µM) treatment; n = 6 ± SD. **B)** MAPK activation upon CEP4 (1 µM) treatment for 10 min. Western blots were probed with α-p44/42. CBB = Coomassie brilliant blue. **C)** RT-qPCR of *FRK1* in seedlings upon CEP4 (1 µM) or ddH_2O treatment for 10 min; n = 3, ± SD. Housekeeping gene *UBQ5*. **D)** MAPK activation upon CEP4 (1 µM) treatment for 10 min. Western blots were probed with α-p44/42. CBB = Coomassie brilliant blue. **E)** $[Ca^{2+}]_{cyt}$ kinetics in seedlings upon CEP4 treatment (1 µM); n = 6, ± SD. **F)** RT-qPCR analysis of *FRK1* in seedlings upon CEP4 (1 µM) or ddH_2O treatment for 4 h; n = 3 ± SD. Housekeeping gene *UBQ5*. **G)** Relative fresh weight of five-day-old seedlings treated with CEP4 (1 µM) for seven days; n = 48 pooled from four experiments ± SD (one-way ANOVA, Tukey post-hoc test, a-b/c/bc $p<0.0001$, b-c $p<0.05$). **H)** $[Ca^{2+}]_{cyt}$ kinetics in seedlings upon CEP1 (10 µM) treatment; n = 4, ± SD. **I)** CEP4, **J)** PIP1 and **K)** CEP1 (**K**) were titrated into a solution containing CEPR2^{ECD} in ITC cells. Top: raw data thermogram; bottom: fitted integrated ITC data curves. **I)** ITC table summarizing RLK7^{ECD} vs CEP4/PIP1/CEP1 as mean ± SD of two experiments. K_d indicates receptor-ligand binding affinity. N indicates reaction stoichiometry. **M)** NLS-3xmVenus signal in p*RLK7*::*Venus-H2B*. Cyan-dotted line represents vasculature. BF = bright field, PI = propidium iodide, scale bar = 100 µm. Different symbols in **C** and **F** represent three independent experiments. Experiments in **A-H**, **M** and **I-K** were repeated at least three times in independent biological repeats or in two independent technical repeats, respectively, with similar results.

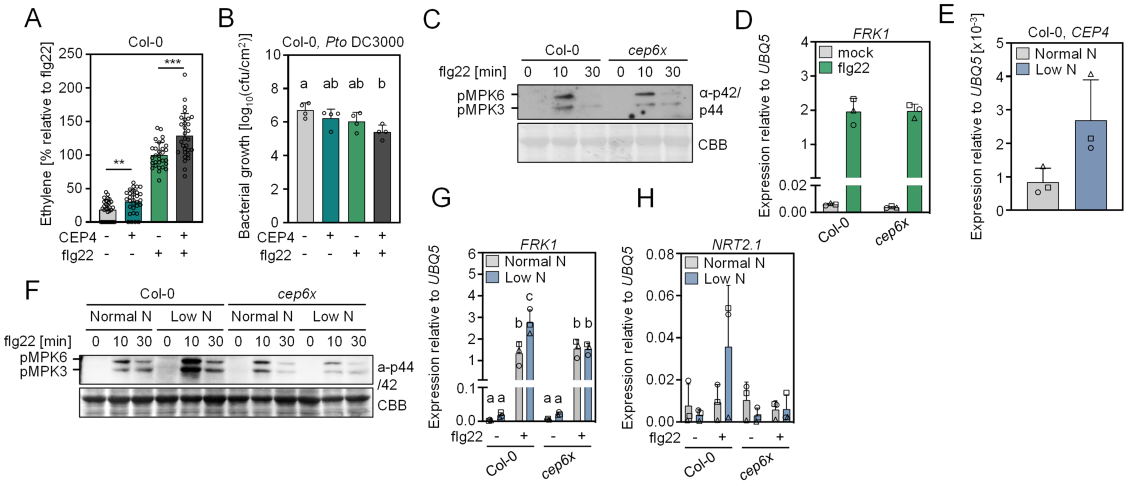

Figure 4: CEPs promote FLS2 signaling during N starvation. A) Ethylene concentration in Col-0 leaf discs 3.5 h after CEP4 (1 µM) and/or flg22 (500 nM) treatment; n = 30, seven pooled experiments ± SD (two-tailed Student's t-test, ** p<0.05, *** p = 0.0001). **B)** cfu of *Pst* DC3000 (3dpi) in Col-0 leaves upon ddH_2O, CEP4 (1 µM) and/or flg22 (100 nM) pretreatment; n = 4 ± SD (one-way ANOVA, Tukey post hoc, a-b p<0.05). **C)** MAPK activation upon flg22 (100 nM) treatment. Western blots were probed with α-p44/42. CBB = Coomassie brilliant blue. **D)** RT-qPCR of *FRK1* upon flg22 (100 nM) treatment for 4 h; n = 3 ± SD. Housekeeping gene *UBQ5* **E)** RT-qPCR of *CEP4* after 24 h transfer of Col-0 seedlings to normal N/low N medium (NN/LN); n = 3 ± SD. Housekeeping gene *UBQ5*. **F)** MAPK activation upon flg22 (100 nM) treatment after 24 h transfer of seedlings to NN or LN. Western blots were probed with α-p44/42. CBB = Coomassie brilliant blue. **G)** RT-qPCR of *FRK1* upon flg22 (100 nM) treatment for 4h after 24 h transfer of seedlings to NN or LN; n = 3 ± SD. Housekeeping gene *UBQ5*; n = 3 ± SD (one-way ANOVA, Tukey post hoc, a-b p<0.01, b-c ≤ 0,001, a-c <0.0001). **H)** RT-qPCR of *NRT2.1* upon flg22 (100 nM) treatment of seedlings for 4h after 24 h transfer to NN or LN; n = 3 ± SD. Housekeeping gene *UBQ5*. Different symbols in figure **D**-**E** and **G**-**H** represent independent biological experiments. All experiments were repeated at least three times in independent biological repeats with similar results.

655 **Supplementary figures**

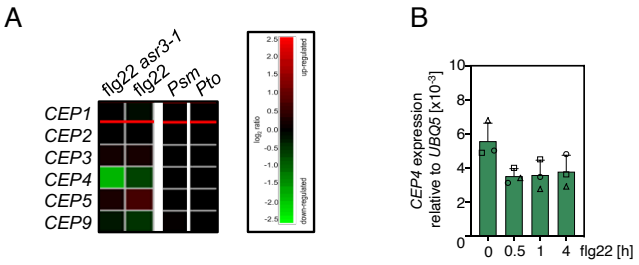

656

657 **Figure S1: CEP4 expression is differentially regulated after flg22 perception.**

658 **A)** *CEP4* is downregulated after flg22 treatment. Data were obtained using Genevestigator software and
659 are based on the AT_mRNASeq_ARABI_GL-1 data set. **B)** *CEP4* expression in roots is weakly
660 downregulated after flg22 treatment. Col-0 seedlings were treated with flg22 (100 nM) for the indicated time
661 after which roots were harvested for RT-qPCR analysis of *CEP4* abundance. Expression of *CEP4* was
662 normalized to *UBQ5*. Different symbols represent three independent experiments ± SD.

663

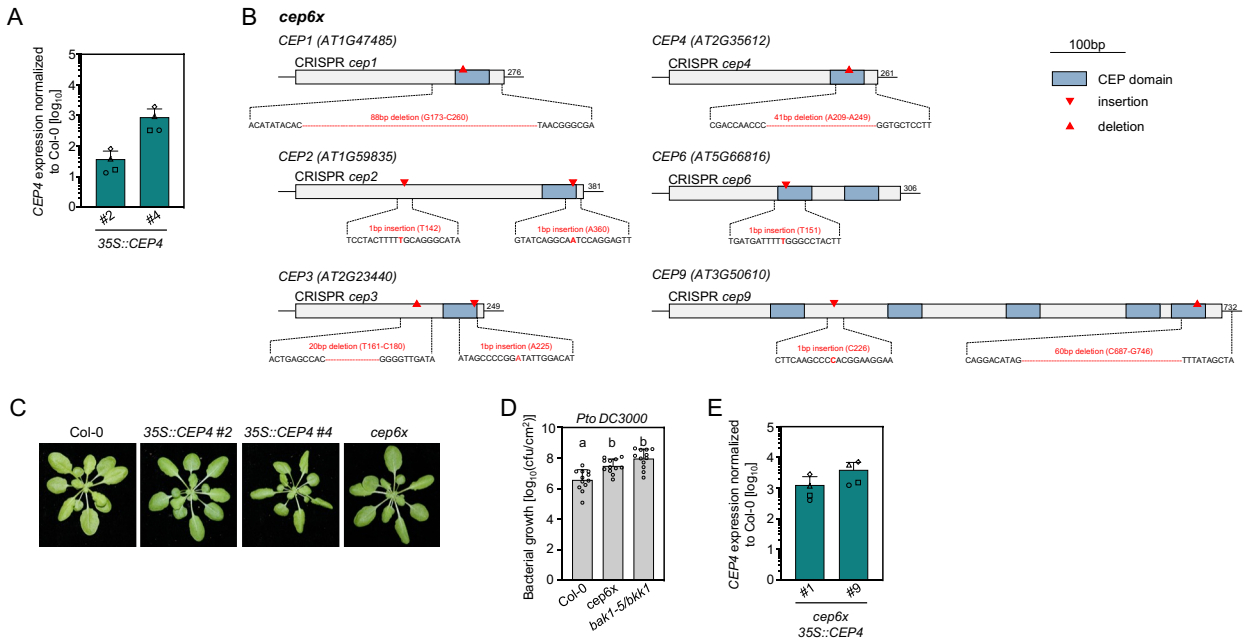

Figure S2: Characterization of *35S::CEP4*, *cep6x* and *cep6x 35S::CEP4*.

A) *CEP4* transcript levels in two independent *CEP4* overexpression lines. Expression of *CEP4* was normalized to *UBQ5* and is shown as a fold induction compared to Col-0. **B)** Characterization of *cep6x*. Schematic diagram of *CEP1*, *CEP2*, *CEP3*, *CEP4*, *CEP6* and *CEP9* gene structure and the CRISPR-Cas9-mediated mutation pattern detected by DNA sequencing. CRISPR *cep1* has an 88 bp deletion including the mature peptide sequence which is indispensable for CEP activity. CRISPR *cep2* mutations show two 1 bp insertions. The first insertion causes a frameshift mutation and leads to an early stop codon before the mature peptide sequence. CRISPR *cep3* has a 20 bp deletion followed by a 1 bp insertion. The mutations lead to an early stop codon before the mature peptide sequence. CRISPR *cep4* has a 41 bp deletion which partially cuts out the coding sequence of the mature peptide. CRISPR *cep6* has a 1 bp insertion which leads to a frame-shift mutation and premature stop codon before the peptide sequence. CRISPR *cep9* includes a 1 bp mutation between CEP9.1 and CEP9.2 sequences which leads to an early stop codon, followed by a 60bp deletion starting in the coding sequence of CEP9.5. The specific location and type of mutations for each gene are indicated in the schematics describing the mutants. **C)** Pictures of 5-week-old plants of the indicated genotypes grown on soil; scale bar = 2 cm **D)** Loss of *CEPs* increases Arabidopsis susceptibility to *Pto* DC3000. Bacterial titer three days after leaf spray infection; n = 12 pooled from three experiments ± SD (one-way ANOVA, Tukey post-hoc test, a-b, $p<0.005$). **E)** *CEP4* transcript levels in two independent lines of *cep6x 35S::CEP4*. Expression of *CEP4* was normalized to *UBQ5* and is shown as a fold change to Col-0. Different symbols in **A** and **E** represent four independent biological repeats ± SD.

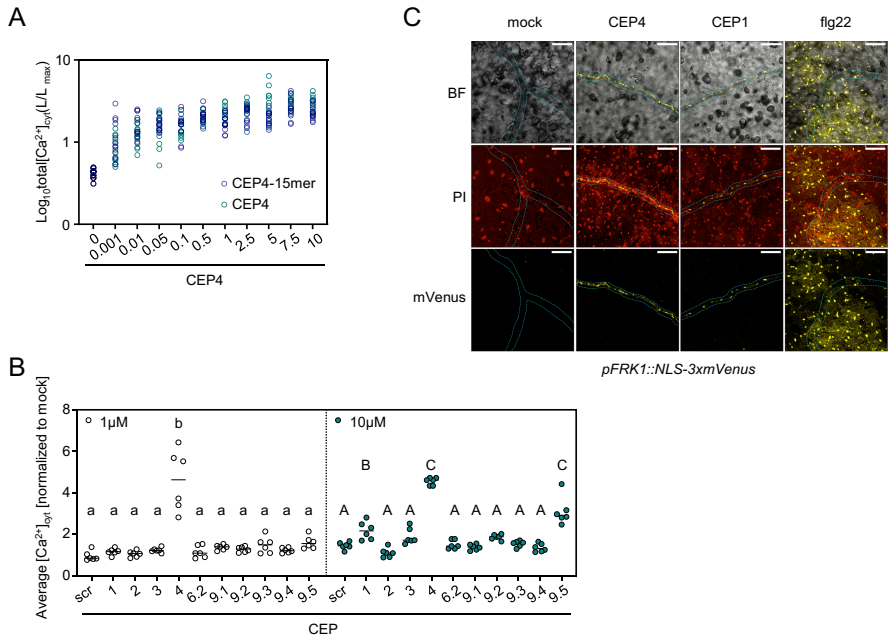

Figure S3: CEP4 is the strongest inducer of PTI responses on the whole tissue level.

A) Both *CEP4* variants trigger influx of calcium ions. Col-0^{AEQ} seedlings were treated with the indicated concentrations of CEP4 and CEP4-15mer. ($[Ca^{2+}]_{cyt}$) was measured for 30 min. Shown is log_{10} of total calcium influx; n = 12 pooled from two experiments. **B)** Some CEPs induce Ca^{2+} influx at higher concentrations. Col-0^{AEQ} seedlings were treated with the indicated concentrations of CEPs. ($[Ca^{2+}]_{cyt}$) was measured for 30 min. The average calcium influx triggered by individual CEPs is normalized to mock (ddH_2O). Dotted line represents different experiments. Statistical analysis was performed separately for each group. Statistical significance was compared to CEP4^{scr} of the indicated concentration; n = 6 (one-way ANOVA, Dunnett post hoc test, a-b $p<0.0001$, A-B $p<0.001$, A-C $p<0.0001$). All experiments were repeated at least three times with similar results. **C)** CEP4 and CEP1 induce *FRK1* promoter activity in the vasculature. Representative images of NLS-3xmVenus signal in *pFRK1::NLS-3xmVenus* lines upon ddH_2O, CEP1 (1 μM), CEP4 (1 μM) or flg22 (10 nM) treatment for 16 h. Maximum projection of Z-stack for mVenus merged with either Z-stacked PI signal or single section BF. Cyan dotted line indicates vasculature. BF = bright field, PI = propidium iodide, scale bar = 100 μm. All experiments were repeated three times in independent biological repeats with similar results.

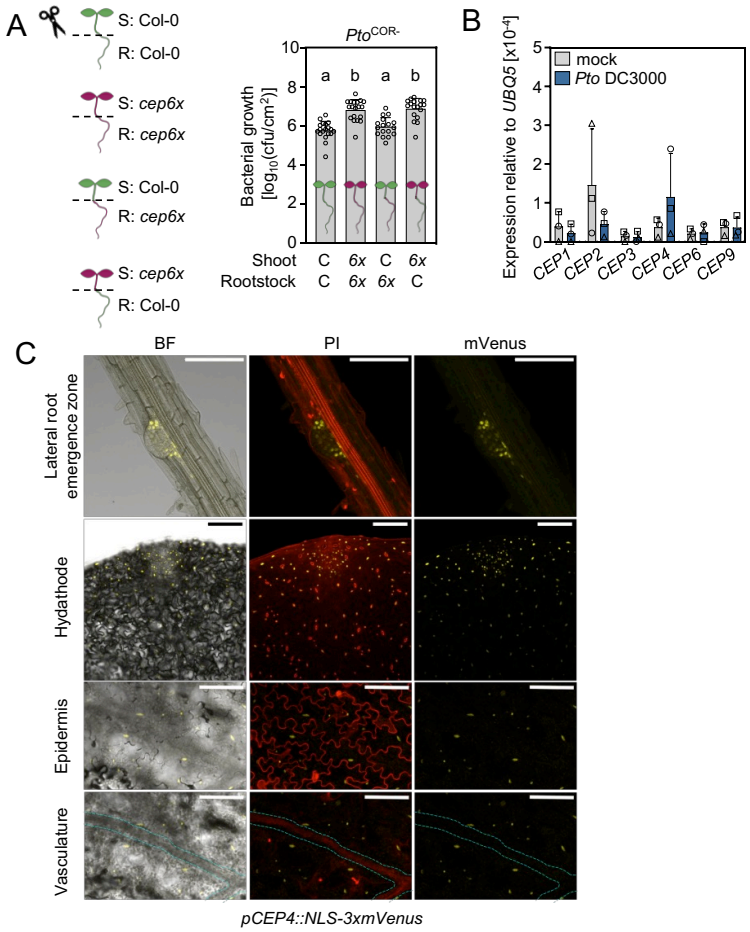

Figure S4: Shoot-expressed *CEPs* are required for basal immunity against *Pto*.

A) Root-expressed *CEPs* are dispensable for resistance to *Pto*$^{COR-}$. Cfu of *Pto*$^{COR-}$ upon spray infection of reciprocally grafted plants. The genotype of the shoot scion is indicated with S, the genotype of the rootstock is indicated with R; n = 17-19 pooled from four experiments ± SD (one-way ANOVA, Tukey post-hoc test, a-b $p<0.0001$). **B)** *CEPs* are weakly expressed in the leaf tissue of adult plants. RT-qPCR analysis of *CEP* expression in ddH_2O and *Pto* DC3000-inoculated leaves 24 h post-treatment; n = 3, ± SD. Housekeeping gene *UBQ5*. **C)** Representative images of *CEP4* promoter activity. For imaging lateral root emergence zone and the hydathode region, maximum projection of Z-stacks for mVenus is merged with either Z-stacked PI signal or single section BF. To show lack of signal mVenus signal in the vasculature, maximum projection of Z-stacks for mVenus is merged with the same single section of PI or BF showing a single epidermal layer or vasculature. Cyan dotted line indicates vasculature. BF = bright field, PI = propidium iodide, scale bar = 100 µm. Different symbols in **B** represent independent experiments. All experiments were repeated at least three times in independent biological repeats with similar results.

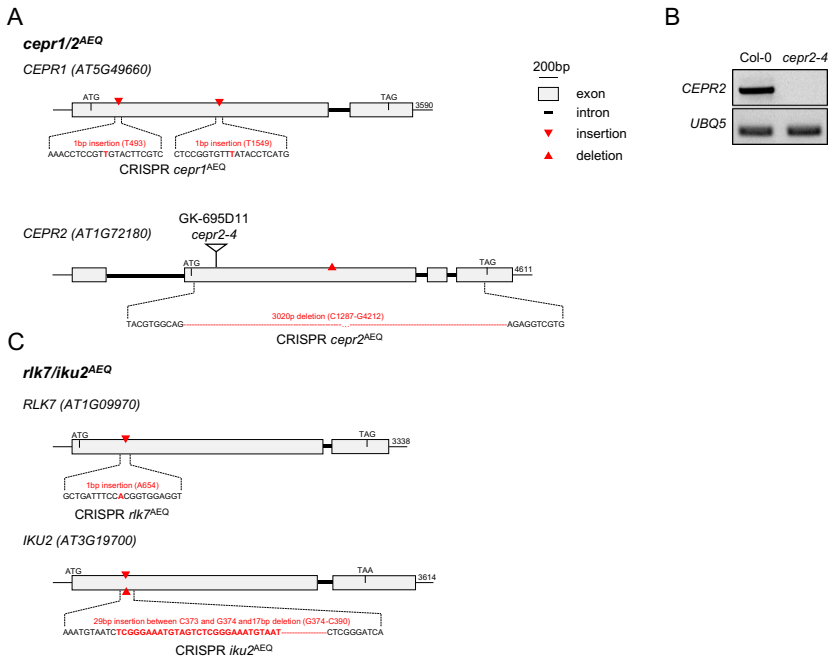

Figure S5: Characterization of *cepr1/2*^{AEQ}, *cepr2-4* and *rlk7/iku2*^{AEQ}.

A) Schematic diagram of the *CEPR1* and *CEPR2* gene structure and the CRISPR-Cas9-mediated mutation pattern detected by DNA sequencing. CRISPR *cepr1* has two 1 bp insertions which lead to a frameshift mutation and an early stop codon. CRISPR *cepr2* has a 3020 bp deletion between the start and stop codon. T-DNA insertion site in *cepr2-4* is indicated. **B)** Characterization of the *cepr2-4* mutant. The *CEPR2* transcript could not be detected in *cepr2-4* mutant in a semi-quantitative RT-PCR analysis. Housekeeping gene *UBQ5*. **C)** Schematic diagram of the *RLK7* and *IKU2* gene structure and the CRISPR-Cas9-mediated mutation pattern detected by DNA sequencing. CRISPR *rlk7* mutant has a 1 bp insertion and CRISPR *iku2* has a 29 bp insertion, followed by a 17 bp deletion. Mutations in both genes lead to a frameshift mutation and an early stop codon. The specific location and type of mutations for each gene are indicated in the schematics describing the mutants.

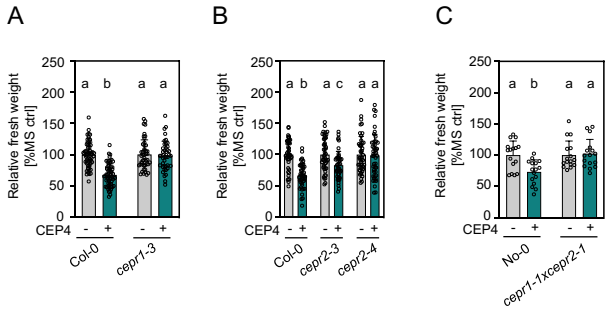

Figure S6: CEPR1 and CEPR2 are similarly required for CEP4-induced seedling growth inhibition. **A)** CEP4-induced seedling growth inhibition is abolished in *cepr1-3*. Relative fresh weight of five-day-old seedlings treated with CEP4 (1 µM) for seven days; n = 42-60 pooled from five experiments ± SD (one-way ANOVA, Tukey post-hoc test, a-b p<0.0001). **B)** CEP4-induced seedling growth inhibition is reduced and abolished in *cepr2-3* and *cepr2-4,* respectively. Relative fresh weight of five-day-old seedlings treated with CEP4 (1 µM) for seven days; n = 46-48 of four pooled experiments ± SD (one –way ANOVA, Tukey post-hoc test, a-b, p<0.0001; c-a/b p<0.05). **C)** CEP4-induced seedling growth inhibition is abolished in *cepr1-1xcepr2-1*. Relative fresh weight of five-day-old seedlings treated with CEP4 (1 µM) for seven days; n=16 ± SD (one-way ANOVA, Tukey post-hoc test, a-b p<0.01). Similar results were obtained in three independent biological repeats.

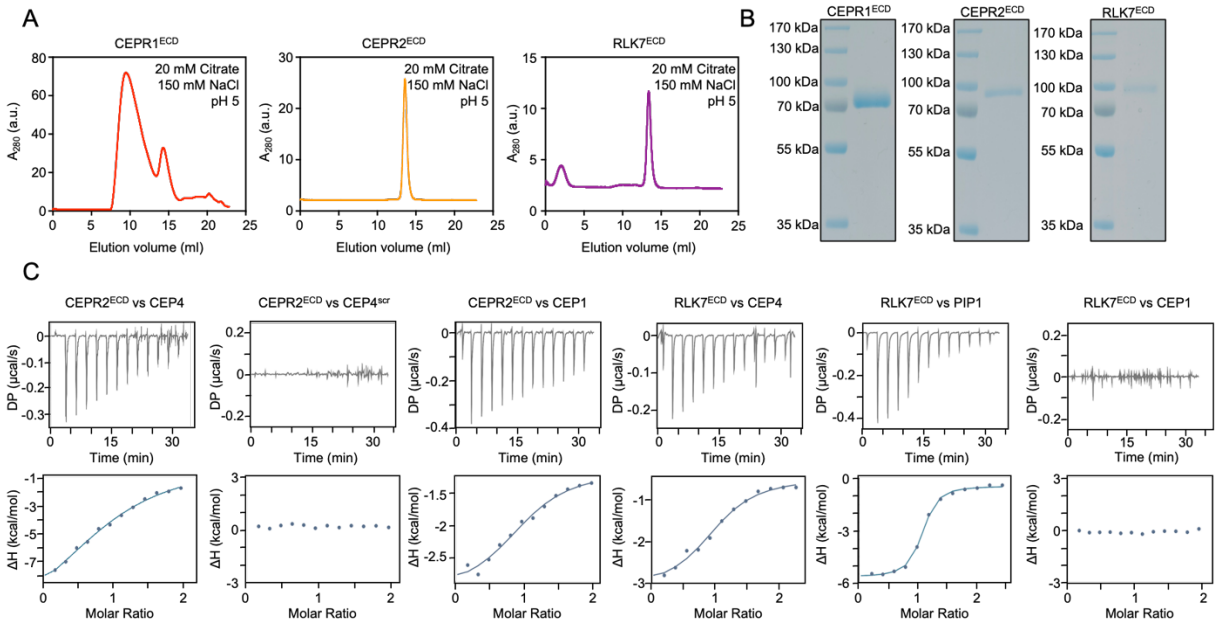

Figure S7: Quality control of recombinant CEPR1, CEPR2 and RLK7 ectodomains and supplemental ITC data.

A) Analytical size-exclusion chromatography (SEC) experiments show $CEPR1^{ECD}$ aggregates in comparison to single peaks for $CEPR2^{ECD}$ and $RLK7^{ECD}$. **B)** SDS-PAGE of the ECD peaks of the SEC analysis in **A**. **C)** ITC thermograms of the second technical repeat performed for each ectodomain and peptide analyzed in Fig. 2 (**E**-**G**) and Fig. 3 (**I**-**K**).

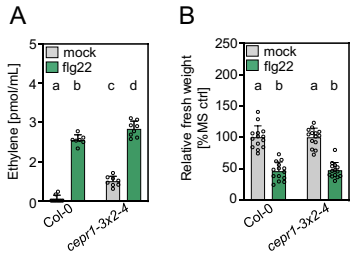

Figure S8: CEPR1 and CEPR2 are dispensable for flg22-induced ethylene accumulation and growth inhibition.

A) Basal and flg22-triggered ethylene production is higher in *cepr1-3/2-4* mutants. Ethylene concentration in leaf discs upon ddH_2O or CEP4 (1 µM) for 3.5 h; n = 7 - 8 pooled from two experiments ± SD (one-way ANOVA, Tukey post-hoc test, a-b/c/d, c-b/d $p<0.0001$, b-d $p<0.005$). **B)** flg22-induced seedling growth inhibition is not affected in *cepr1-3/2-4*. Relative fresh weight of five-day-old seedlings treated with flg22 (100 nM) for seven days; n = 14 ± SD (one-way ANOVA, Tukey post-hoc test, a-b $p<0.0001$). The experiment was performed twice in independent biological repeats with similar results.

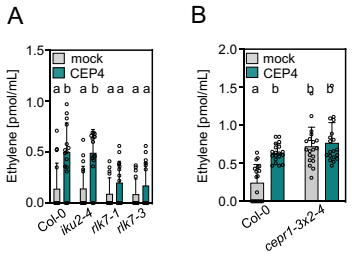

Figure S9: *rlk7* and *cepr1/2* mutants show compromised CEP4-induced ethylene accumulation. **A)** CEP4-triggered ethylene production is reduced in *rlk7* mutants. Ethylene concentration in leaf discs upon ddH_2O or CEP4 (1 µM) treatment for 3.5 h; n = 15 pooled from three experiments ± SD (one-way ANOVA, Tukey post hoc, a-b $p<0.01$). **B)** CEP4-triggered ethylene production is compromised in *cepr1-3/2-4*. Ethylene concentration in leaf discs upon ddH_2O or CEP4 (1 µM) treatment for 3.5 h; n = 19 pooled from four independent experiments ± SD (one-way ANOVA, Tukey post hoc, a-b $p<0.0001$).

Peptide name	Sequence
CEP1	DFRHypTNPGNSHypGVGH
CEP2	DFAHypTNPGDSHypGIRH
CEP3	TFRHypTEPGHSHypGIGH
CEP4^{scr}	TGQHypDHQRHypFAHIGGS
CEP4^{15mer}	AFRHypTHQGHypSQGIGH
CEP4^{16mer}	DAFRHypTHQGHypSQGIGH
CEP6.2	DFEPTTHypGHSHypGVGH
CEP9.1	DFVHypTSHypGNSHypGVGH
CEP9.2	DFAHypTSHypGHSHypGVGH
CEP9.3	DFAHypTSHypGNSHypGIGH
CEP9.4	DFAHypTTHypGNSHypGMGH
CEP9.5	DFKPTTHypGHSHypGVGH
PIP1	RLASGHypSPRGRGH
Flg22	Ac-QRLSTGSRINSAKDDAAGLQIA

770 **Table S1: Peptides used in this study**

771

772

Target site	Sequence	Purpose
CEP1.1	TGGTCACATATACACGGCG	Generation of *cep6x* mutant
CEP1.2	CAGGCGTTGGACACTCTAA	
CEP2.1	GTCCCGGTATCAGGCATCC	
CEP2.2	ATGTATGCCCTGCAAAAGT	
CEP3.1	TACGGAATGTCCAATACCG	
CEP3.2	TATCAACCCCGTGGCTCGG	
CEP4.1	CATTCCGACCAACCCACCA	
CEP4.2	TATTTTAAGGAGCACCTGG	
CEP6.1	ATGATCATCATTTCACAGT	
CEP6.2	TCGGGTACACTGATGATTT	
CEP9.1	CAAGATGACTTCAAGCCCA	
CEP9.2	ACACCAGGACATAGCCCCG	
CEPR1.1	AGAGAGACGAAGTACACGG	Generation of *cepr1/2*^{AEQ} mutant
CEPR1.2	AGCTCATGAGGTATAACAC	
CEPR2.1	GACCTCCTACGTGGCAGCG	
CEPR2.2	CTCAGACCGAGTATGAGAG	
RLK7.1	AGATTGATCTCTCTCGTCG	Generation of *rlk7/iku2*^{AEQ} mutant
RLK7.2	GCGACGGCTGATTTCCCGG	
IKU2.1	GCTTGAGATACTTAGACCT	
IKU2.2	CTTGTTCGTCTACAAAACT	

773 **Table S2: CRISPR-Cas9 target sites.**

774

Primers used for cloning		
Primer name	**Sequence (5'→3')**	**Purpose**
pCEPR1-BsaI-F	GCGCGCGGTCTCTCGAGTCAGTTTTTTT GGATTCAGATTTG	*pro*CEPR1 for pCEPR1::NLS-3xmVenus-tNOS
pCEPR1-BsaI-R	GCGCGCGGTCTCTCATTTTTCAGAGAAA GATCAAAAGTAACC	
pCEPR2-BsaI-F	GCGCGCGGTCTCTCGAGTTTTGTATACT CTTAAAAAAACTATG	*pro*CEPR2 for pCEPR2::NLS-3xmVenus-tNOS
pCEPR2-BsaI-R	GCGCGCGGTCTCTCATTTTATAGTGATT CCCAAGGG	
pCEP4-BpiI-F	TTGAAGACTTCGAGAATATAAACAAATA TAGGTAAC	*pro*CEP4 for pCEP4::NLS-3xmVenus-t35S
pCEP4-BpiI-R	TTGAAGACTTCATTCACTTGACAACTTTC TG	
pRLK7-Attb1	GGGGACAAGTTTGTACAAAAAAGCAGG CTTAGAGCTAAGACATATAACT	*pro*RLK7 for pRLK7-H2B-mVenus
pRLK7-Attb2	GGGGACCACTTTGTACAAGAAAGCTGG GTAGTCGGAGAGAAGAAGTGG	
Primers used for RT-qPCR		
Primer name	**Sequence (5'→3')**	**Purpose**
qUBQ5-F	ACTCCTTCCTCAAACGCTGA	*UBQ5*
qUBQ5-R	CCAAGCCGAAGAAGATCAAG	
qFRK1-F	TGCAGCGCAAGGACTAGAG	*FRK1*
qFRK1-R	ATCTTCGCTTGGAGCTTCTC	
qPR1-F	CGGAGCTACGCAGAACAACT	*PR1*
qPR1-R	CAGACAAGTCACCGCTACCC	
qNRT2.1-F	AACAAGGGCTAACGTGGATG	*NRT2.1*
qNRT2.1-R	CTGCTTCTCCTGCTCATTCC	
qCEP1-F	AATGCTAAAGGGGTGTTTGG	*CEP1*
qCEP1-R	ACAAACCCACGACAAAGACA	
qCEP2-F	TGGTGACCATTTTGACCATC	*CEP2*
qCEP2-R	CCGACCATCTTTTTCGACTT	
qCEP3-F	GACCTACGGAACCTGGTCAT	*CEP3*
qCEP3-R	AAAAAGTCACCAGGCCAATC	
qCEP4-F	AGAATACAAAAGCAGCTCGAC	*CEP4*
qCEP4-R	TCCAATACCTTGACTAGGACC	
qCEP6-F	GTCGGGTAATCTAGACCTTCCTC	*CEP6*
qCEP6-R	CGGTTTTTCGCAACTGTCTCG	
qCEP9-F	AGCTGGATTTACAGATGATTTCG	*CEP9*
qCEP9-R	TGTCCCACACCAGGACTGT	
Primers used for genotyping and sequencing		
Primer name	**Sequence (5'→3')**	**Purpose**
GG pUC18 Seq-F	GTATCACGAGGCCCTTTCGT	Inserts in GoldenGate pUC18
GG pUC18 Seq-R	TAATGAATCGGCCAACGC	
CEP1-CRISP-s1	CCTTGTTTTGTTTTACATATTCTT	CRISPR CEP1
CEP1-CRISP-s2	TCTGAATGAAAATACATGTAATTTTC	
CEP2-CRISP-s1	CATTCAATACTTCTCATATACAAAAC	CRISPR CEP2
CEP2-CRISP-s2	TCACCAGTTTTCTTTAGTCTTC	
CEP3-CRISP-s1	CATTTTCGCCTTCGACTA	CRISPR CEP3
CEP3-CRISP-s2	CAATCATATTTTCAACATGTAATCAC	
CEP4-CRISP-s1	GACATACGCTTTTAAAGGAAG	CRISPR CEP4
CEP4-CRISP-s2	GAAGAACTGTGTGCGATAAAG	
CEP6-CRISP-s1	CCTCTCTCGTATACACTAGAAAC	CRISPR CEP6
CEP6-CRISP-s2	TTAATTTAGCAAAAGCATTGAAG	
CEP9-CRISP-s1	ATATATACAAACTCCTAAACCTTGC	CRISPR CEP9

CEP9-CRISP-s2	CATATCGTAAACCAATGTATTAGA	
CEPR1-CRISP-s1	CGTAAGATGTGACGGTCAA	CRISPR CEPR1
CEPR1-CRISP-s2	GGTTGCCTTGCAGTACAA	
CEPR2-CRISP-s1	GAATTCCAGTGCATCGACC	CRISPR CEPR2
CEPR2-CRISP-s2	CTAAAACGTGGTAGGTGAATCAT	
RLK7-CRISP-s1	TCAAACCACCGTCACCACTT	CRISPR RLK7
RLK7-CRISP-s2	TCCAAATTCCGAAGCTCCGT	
IKU2-CRISP-s1	GCATGTGAATTCGCCGGAAT	CRISPR IKU2
IKU2-CRISP-s2	CCGCAGCTCTGATAAATCACC	
pCEPR1-s1	CTAGTCACCTGCAGCTCG	pCEPR1
pCEPR1-s2	GTGTAGTTCACGTCGGATG	
pCEPR1-s3	CAAACGCTTCACTTATGTAATG	
pCEPR1-s4	GCATCTATCTGATTCTGATCGTG	
pCEPR1-s5	CATCCGACGTGAACTACAC	
pCEPR2-s1	ACGACAATCTGAGCTCCAC	pCEPR2
pCEPR2-s2	TGGGATTCGGAGCATAAGG	
pCEPR2-s3	TCCATCTAGAAACATTAACCGA	
pCEPR2-s4	CCTAGAACGTGGTCCAAG	
pCEPR2-s5	CTGCACTGTAATGAGTACC	
pCEPR2-s6	CGGTAATAGATAGTGAAATGG	
cepr1-3-LP	TAAATCAAGAATCCACTTCCATGC	*cepr1-3*
cepr1-3-RP	CCTAATGGTAACTTATGGGACGCT	
cepr2-4-LP	GGTGAGTTCGTTATCGCTGAG	*cepr2-4*
cepr2-4-RP	AATGTTGAATCGACCGTTGAG	
GABI_o8474	ATAATAACGCTGCGGACATCTACATTTT	T-DNA primer for GABI-kat
cepr2-3-LP	TCACAACTCTGTAACGCAACG	*cepr2-3*
cepr2-3-RP	AACTCGGAGTTTTGAAGGAGC	
rlk7-1-LP	CCGCCTCTCTCTCTCTCTCTC	*rlk7-1*
rlk7-1-RP	AAGCAGAGCTTTCATCTTCCC	
rlk7-3-LP	ACGATTTGATCGTCGTGCTAC	*rlk7-3*
rlk7-3-RP	TTACAACAACTCCTTGACCGG	
iku2-4-LP	TCTTTAAGAACCGCAGCTCTG	*iku2-4*
iku2-4-RP	GTTGTTTCGCCTACAATGACC	
LBb1.3	ATTTTGCCGATTTCGGAAC	T-DNA LB primer for *rlk7-1, rlk7-3, iku2-4*
LBb1	GCGTGGACCGCTTGCTGCAACT	T-DNA LB primer for *cepr2-3*

775

776 **Table S3: Primers used in this study.**

777

778

779

780